1-1-2012

A Role For Reactive Oxygen Species In Photodynamic Therapy

Michael Price
Wayne State University,

A ROLE FOR REACTIVE OXYGEN SPECIES IN PHOTODYNAMIC THERAPY

by

MICHAEL PRICE

DISSERTATION

Submitted to the Graduate School

of Wayne State University,

Detroit, Michigan

in partial fulfillment of the requirements

for the degree of

DOCTOR OF PHILOSOPHY

2012

MAJOR: CANCER BIOLOGY

Approved by:

_____

Advisor Date

_____

_____

_____

_____

DEDICATION

I dedicate this work to my family, whose support got me through my studies and work. I would also like to thank all the teachers and professors from my past who instilled the meaning of hard work and dedication to learning in me. Most of all I would like to thank my wife, Aimee, and my son, Thadeus, not only all their support and motivation but especially for their endless patience with me in this endeavour.

ACKNOWLEDGEMENTS

I would like to acknowledge Dr. David Kessel, my mentor, not just for the help and support in my graduate studies but most importantly for his guidance in my development and maturity as a researcher.

I would next like to give my deepest appreciation and gratitude to Ann Marie Santiago, a research assistant in Dr. Kessel's laboratory. She taught me many valuable techniques and assisted me on many experiments in the lab. To my fellow Cancer Biology students and the program faculty I would like to give many thanks for their support and encouragement over the years. I would also like to thank Drs. Rasheeda Zafar and Joseph Dunbar for their invaluable mentorship.

Finally, I would like to acknowledge the members of my dissertation committee for all the guidance and encouragement they gave me throughout the years on my dissertation. My greatest appreciation to Drs. Stanley Terlecky, John Reiners Jr., Raymond Mattingly, and Hyeong-Reh Kim.

TABLE OF CONTENTS

LIST OF TABLES

LIST OF FIGURES

LIST OF ABBREVIATIONS

APF	3'(*p*-aminophenyl) fluorescein
3-AT	3-amino-1,2,4-triazole
BIP	2,2'-bipyridyl
BPD	benzoporphyrin derivative (Verteporfin)
CAT_{SKL}	catalase-$_{SKL}$
CCD	charged couple device
ClO^-	hypochlorite ion
CPO	9-capronyloxy-tetrakis(methoxyethyl) porphycene
DADB	diethyl-3-3'-(9,10-anthracenediyl)bis acrylate
DAF	4',5'-diaminofluorescein
DCF	2',7'-dichlorofluorescein
DEANO	diethylamine nitric oxide
DFO	desferroxamine
DHE	dihydroethidine
DHR	dihydrorhodamine
DMSO	dimethyl sulfoxide
ER	endoplasmic reticulum
ESR	electron spin resonance
$Fe(NH_4)SO_4$	ferrous ammonium sulfate (FAS)
H_2O_2	hydrogen peroxide
H_2SO_4	sulfuric acid
HA14-1	2-amino-6-bromo-α-cyano-3-(ethoxycarbonyl)-4*H*-1-benzopyran-4-acetic acid ethyl ester
HIF1-α	hypoxia inducible factor1-alpha
HO33342	Hoechest dye 33342

HPF	3'(*p*-hydroxyphenyl) fluorescein
HPD	hematoporphyrin derivative
HRP	horseradish peroxidase
KO_2	potassium superoxide
LDL	low density lipoprotein
LuTex	lutetium texaphyrin
mTHPC	meta(tetrahydroxyphenyl)chlorin (Foscan)
NPe6	mono-L-aspartyl chlorin e6
$^1O_2$	singlet oxygen
$\bullet O_2^-$	superoxide anion
$ONOO^-$	peroxynitrite ion
•OH	hydroxyl radical
PDT	photodynamic therapy
Pc4	phthalocyanine 4
RNS	reactive nitrogen species
ROS	reactive oxygen species
RPCI	Roswell Park Cancer Institute
SnET2	tin etiopurpurin
SOD	superoxide dismutase
SOSG	singlet oxygen sensor green
$TiOSO_4$	titanium oxysulfate
TMPyP	5,10,15,20-tetrakis (*N*-methyl-4-pyridyl)-21*H*,23*H*
TPPS	porphine tetra(*p*-phenylsulfonate)

CHAPTER 1 - INTRODUCTION

1.1 PHOTODYNAMIC THERAPY: INTRODUCTION AND BACKGROUND

The term ‘photodynamic therapy’ was invented in the early 1900s by Hermann von Tappeiner. This relates to the ability of reactive oxygen species, formed during irradiation of ‘photosensitizers’ to exert lethal effects on living cells. The process involves an interaction between light, oxygen and a chemical compound with appropriate photochemical properties and structure. The effect had been known for centuries; one of the earliest uses of a photodynamic effect had been the use of light for the bleaching of linen, a process that can be traced back to the early Egyptians, Indians, and Chinese over thirty centuries ago (Dolmans, Fukumura et al. 2003; Moan and Peng 2003). The ability of certain dyes to sensitize microorganisms to light was first reported by Oscar Raab, a medical student at the Pharmacological Institute of Munich, in 1900 (Dolmans, Fukumura et al. 2003). This phenomenon was periodically re-discovered during the next 50 years, but the modern era of photodynamic therapy, as a procedure for cancer therapy, did not begin until 1960 (Dougherty, Gomer et al. 1998). Sam Schwartz and Richard Lipson, two physicians at the Mayo Clinic, had begun a study of the ability of a crude hematoporphyrin preparation to localize in neoplastic tissues, as determined by fluorescence under ultraviolet light. Schwartz later empirically developed an optimized formulation based on the treatment of crude hematoporphyrin with a mixture of acetic and sulfuric acids, followed by neutralization. He termed the product "hematoporphyrin derivative" (HPD). This turned out to be a superior tumor-localizing product, but there was little progress until the work of Thomas Dougherty's group at the Roswell Park Cancer Institute (RPCI) in the early 1970s.

Dougherty was exploring a series of agents proposed to be radiation sensitizers.

During the course of this work, he consulted with Dr. Schwartz who reported that porphyrins could sensitize malignant cells and tissues to both radiation and light. Dougherty persuaded a group of physicians at RPCI to initiate a collaborative project involving the potential use of HPD + light for cancer control. This work resulted in evidence that HPD administered to tumor-bearing animals or cancer patients, localized at tumor sites. When these sites were irradiated with red light (~630 nm), a selective tumor destruction/shrinkage resulted. This work attracted the attention of other local surgeons and ultimately led to the use of photodynamic therapy (PDT) worldwide. It was found that PDT eradicates tumors by both direct cell killing and shutdown of the tumor vasculature. This latter finding ultimately led to one of the early major successes in the field of PDT: the use of a photosensitizing agent for the treatment of macular degeneration (Dougherty, Gomer et al. 1998). This is a common condition, leading to impaired vision, resulting from a proliferation of blood vessels in the eye.

The protocol termed ‘PDT’ involves the use of three components; a photosensitizing agent that is harmless in the absence of light, a light source that is used to ‘activate’ the drug but is otherwise harmless, and dissolved molecular oxygen in the tissue/cells (Dougherty, Gomer et al. 1998; Agostinis, Berg et al. 2011). The wavelength of light for activation must correspond to an absorbance band of the photosensitizer being used. This can vary as a function of the chemical structure of the photosensitizing agent. The optimal wavelength for clinical efficacy is in the red or near infrared, since these wavelengths penetrate tissues most effectively. Shorter wavelengths of light are scattered by tissues and their penetration is severely limited. It has been estimated that, under ideal conditions, light in the vicinity of 650-700 nm can penetrate to a depth of at least one centimeter. Absorption of a photon leads to the

formation of an 'excited state' of the photosensitizing agent. When this energy is lost as the photosensitizer returns to ground state, three different effects can occur. The absorbed energy can be lost as heat or released in the form of light, emitted at a longer wavelength (fluorescence). The excess energy can also be transferred to another molecule. When this involves oxygen, there can be a charge-transfer reaction that initially results in formation of a series of oxygen and other radical species. This is termed a 'Type I' reaction. An energy-transfer (Type II) can also occur (Foote 1991). This results in the alteration of the spin of a single electron, resulting in formation of a highly reactive oxygen molecule: singlet oxygen ($^1O_2$). Singlet oxygen can catalyze oxidation of any nearby biological species, often with cytotoxic consequences. It should be noted that the fluorescence of the photosensitizer can also be used for tumor localization if an appropriate detection system is available.

The first oxygen radical formed is most often superoxide anion ($\bullet O_2^-$). This species is converted both spontaneously and by the action of superoxide dismutase (SOD) to hydrogen peroxide (H_2O_2), a molecule with a much longer half-life than other reactive oxygen species (ROS). Hydrogen peroxide can, unlike other ROS, pass through biological membranes and cause damage in other cellular compartments (Plaetzer, Krammer et al. 2009). Hydrogen peroxide is detoxified by the enzyme catalase, resulting in formation of $H_2O + O_2$. Hydrogen peroxide can also be converted to a highly reactive product, the hydroxyl radical ($\bullet OH$), via the Fenton reaction and other processes. The Fenton reaction involves the catalytic action of metal ions, e.g., Fe^{+2}, but this reaction can also be mediated by certain enzymatic processes.

Both Type I and Type II reactions can occur simultaneously, with the ratio between these processes depending on the photosensitizer, as well as the

concentrations of substrate and oxygen (Castano, Demidova et al. 2004; Plaetzer, Krammer et al. 2009). Because of the high reactivity and short half-life of singlet oxygen and the oxygen radicals, only molecules and structures that are proximal to the site(s) of their production, i.e. sites of photosensitizer localization, are subject to PDT phototoxicity.

Two factors promote the selectivity of PDT. For reasons not yet completely understood, some photosensitizing agents show affinity for tumors and their vasculature. Moreover, the photosensitizers are inactive until irradiated. This is an important consideration since sensitizers often partition to the liver and spleen. Since these sites can be shielded from light, they are spared from toxicity. Because of the high degree of specificity allowed by this therapy, adverse effects associated with conventional chemotherapy are absent when PDT is used. The reactive singlet oxygen species has a very short half-life, restricting photodamage to a < 20 nm region from the site of formation (Moan and Berg 1991). The cytotoxic effect of PDT is therefore confined to close proximity of the tumor site, resulting in minimal destruction of normal tissue upon irradiation. Light delivery by means of lasers coupled to fiber cables permits selective exposure of sites to irradiation, as to also spare damage to surrounding normal tissue (Sibata, Colussi et al. 2000).

In the clinical setting, PDT can be used as a single agent for treatment of cancer or can be combined with other antitumor treatments without the risk of inducing cross-resistance. PDT can also be used in combination with surgery using fluorescence-guided illumination to eradicate malignant lesions (Allison, Downie et al. 2004). It is also feasible to irradiate the tumor bed after resection to eradicate residual tumor. PDT has been successfully combined with radiotherapy and chemotherapy (Sibata, Colussi

et al. 2000; Agostinis, Berg et al. 2011). It has been observed that PDT can promote responses in malignant lesions that are resistant to drugs and ionizing radiation (Cuenca, Allison et al. 2004). Drug resistance occurs when malignant cells develop mechanisms that allow them to survive in the presence of chemotherapy. PDT can bypass drug resistance pathways because phototoxicity involves triggering the late stages of apoptosis, avoiding defective signalling pathways often found in neoplastic cells.

PDT is currently being used in the treatment of several types of cancers including basal cell carcinomas, early carcinomas of the oral cavity, pharynx, larynx, and esophagus preserving normal tissue and vital functions of speech and swallowing. Cancers of the GI, lung, bladder, and brain have also been successfully treated with PDT (Agostinis, Berg et al. 2011). In the treatment of cancer patients, PDT holds several advantages over the three primary modes of cancer therapy used today (surgery, chemotherapy, and radiation); a) in being minimally invasive and requiring only illumination of the tumor tissue, the treatment of irresectable tumors is possible. b) PDT can be repeated without detrimental consequences to the patient; c) the therapy does not result in systemic immunosuppressive effects which can lead to possible infections (Robertson, Evans et al. 2009). An obvious consideration is that the site(s) of neoplasia need to be known so that light can be directed to the appropriate sites.

Several explanations have been suggested for the preferential binding of sensitizers to neoplastic tissues: low tumor pH, elevated LDL (low density lipoprotein) receptor expression, poorly developed lymphatic drainage, and abnormal tumor neovascularization. Some photosensitizers are known to bind to LDL and are thereby directed to malignant cells that often express high levels of LDL receptors. There are,

however, sensitizers that bind high-density lipoproteins, e.g., NPe6 (mono-L-aspartyl chlorin e6), and LuTex (lutetium texaphyrin), so there appear to be multiple determinants of localization (Hamblin and Newman 1994; Dougherty, Gomer et al. 1998; Castano, Demidova et al. 2005).

Many porphyrin molecules and analogs have been identified that can induce photodynamic cell death. Photosensitizers can localize in mitochondria, ER (endoplasmic reticulum), lysosomes, plasma membrane and even the nucleus (Castano, Demidova et al. 2004). One group of effective photosensitizers, represented by CPO [9-capronyloxy-tetrakis(methoxyethyl) porphycene] and mTHPC [meta-(tetrahydroxyphenyl)chlorin], localize at the ER and catalyze photodamage to the anti-apoptotic molecule Bcl-2, leading to a rapid apoptotic response. Oleinick's group reported that the photosensitizer phthalocyanine 4 (Pc4), a mitochondrial photosensitizer, also causes Bcl-2 photodamage (Xue, Chiu et al. 2001). The tin etiopurpurin (SnET2) localizes in both the mitochondria and lysosomes (Kessel, Luo et al. 1997), but the predominant effect of the sensitizer appears to be on Bcl-2. Effects associated with Bcl-2 photodamage include loss of protection by this anti-apoptotic protein. This leads to a decreased mitochondrial membrane potential, increased mitochondrial membrane permeability and cytochrome c release. The appearance of cytochrome c in the cytoplasm is a trigger for the irreversible process of apoptosis, initiated by caspase-3 activation.

Another group of photosensitizers, represented by the chlorin NPe6, LuTex, and the bacteriochlorin analog WST11, targets lysosomes. Other photosensitizing agents localize in the plasma membrane where irradiation leads to necrosis via membrane photodamage (Dougherty, Gomer et al. 1998; Allison, Downie et al. 2004). The cationic

porphyrin, 5,10,15,20-tetrakis (*N*-methyl-4-pyridyl)-21*H*,23*H* porphyrin (TMPyP) has an unusual mode of photodynamic action; it localizes to the nuclei and irradiation leads to damage to guanine residues in DNA, triggering apoptosis (Tada-Oikawa, Oikawa et al. 2009).

1.1.1 Apoptosis

Apoptosis is an important process for maintaining a balance between growth and death, and in embryonic development. In malignant cells, apoptosis is often suppressed or defective, allowing uncontrolled cell proliferation. Apoptosis has been described as a system of 'programmed cell death' that can involve extrinsic or intrinsic pathways. Both pathways involve the mitochondrion and several membrane-bound and cytosolic proteins. The program is mediated by a cascade of events that ultimately leads to irreversible caspase activation and cell fragmentation. Caspases are cysteine proteases that are inactive until activated by apoptotic signal (Nunez, Benedict et al. 1998). The caspases are characterized as initiators (caspases-8 and -9) or executioners (caspases-3, -6, -7) (Grutter 2000). Activation of initiator caspases leads to executioner caspase activation and irreversible cell death. Typical morphological characteristics of apoptosis are DNA fragmentation into endonucleosomes, cell shrinkage, membrane blebbing, intact organelles and formation of apoptotic bodies. The anti-apoptotic proteins Bcl-2 and Bcl-xL are targets for some photosensitizing agents, i.e., when mitochondria or the ER are PDT targets (Kim, Luo et al. 1999; Xue, Chiu et al. 2001). The loss of Bcl-2 will almost invariably trigger an apoptotic response.

A second mechanism for the photodynamic triggering of apoptosis involves the release of proteases from photodamaged lysosomes. These enzymes can cleave the pro-apoptotic protein Bid to form a truncated form (t-Bid) that can directly interact with

mitochondria and promote release of cytochrome c and the initiation of apoptosis (Reiners, Caruso et al. 2002).

1.1.2 Necrosis

Necrosis can occur when the degree of photodamage is so great that enzymes needed for the apoptotic process are destroyed. Such a high dose of light and/or drug will generally lead to loss of PDT selectivity since a low concentration of photosensitizers is often found in normal tissues (He and Oleinick 1995; Luo and Kessel 1997). Moreover, necrosis can lead to the release of tumor DNA into the circulation–a process with possibly adverse consequences.

1.1.3 Autophagy

Photodamage can also lead to the initiation of autophagy. This process involves the formation of vacuoles (autophagosomes) that engulf cellular components (intracellular proteins and organelles). This is most often associated with starvation conditions where cells recycle a portion of their components to remain viable. The process concludes with the fusion of the outer membranes of autophagosomes and with lysosomes. Hydrolases and lipases in the lysosomal lumen then degrade the autophagic contents, with the resulting amino acids, fatty acids, and nucleosides released back into the cytosol for reutilization by the cell (Levine and Klionsky 2004; Gozuacik and Kimchi 2007; Yang and Klionsky 2009; Wirawan, Vanden Berghe et al. 2012). While autophagy is usually considered as a pro-survival mechanism, if autophagy becomes excessive, it may lead (or be associated with) to cell death (Kessel and Oleinick 2009). It is not yet clear whether autophagy is actually a death mechanism. Some authors prefer to use the term ‘death with autophagy’ (Kroemer and Levine 2008), suggesting that death arises by other mechanisms that can also evoke an

autophagic response. It is important to consider that Bcl-2 is also an anti-autophagic protein. It forms a complex with the pro-autophagic protein Beclin-1. Any process leading to the loss Bcl-2 could therefore trigger autophagy (Pattingre and Levine 2006).

1.1.4 Induction of cell death by PDT

A mechanism for PDT-induced cell death can therefore be proposed. Photodamage to Bcl-2 or activation of Bid leads to initiation of apoptosis and cell death. Evidence that autophagy can offer protection from PDT has been provided by Oleinick's group (Xue, Chiu et al. 2008) and by the finding that inhibition of autophagy promotes PDT efficacy. When autophagy was limited by a knockdown of a critical autophagy gene (Atg7), the 'shoulder' on the dose response curve was lost, indicating a role of autophagy in promoting survival at low PDT doses (Andrzejak, Price et al. 2011). In a recent study, it was shown that the photosensitizer BPD could inhibit autophagy at high concentrations in the dark (Donohue, Tovey et al. 2011). When conditions were modified so that there was a higher drug dose and a correspondingly lower light dose, the result was also the loss of this 'shoulder', again demonstrating the ability of autophagy to offer some protection from photokilling (Andrzejak, Price et al. 2011). This result also suggested a potential for use of high-dose BPD as a means of promoting PDT efficacy, with the light-dose appropriately reduced.

1.2 HYPOTHESIS

With the possibility that both Type I and II reactions can occur in parallel, the *particular* reactive oxygen species being formed during the irradiation process can be an important determinant of PDT efficacy. Having a better understanding of the pathways of ROS formation can therefore aid in analyzing PDT mechanisms. This can be accomplished through the use of agents that inhibit or facilitate ROS formation

(Figure 1.1). These data are important due to the distinct properties of each ROS, including lifetime, diffusion distance and reactivity. Effects of the level of oxygenation were examined on efficacy of two agents that form different ROS upon irradiation. The results indicate that PDT efficacy can be affected by the nature and persistence of ROS formed when the excited state of a photosensitizer interacts with dissolved oxygen.

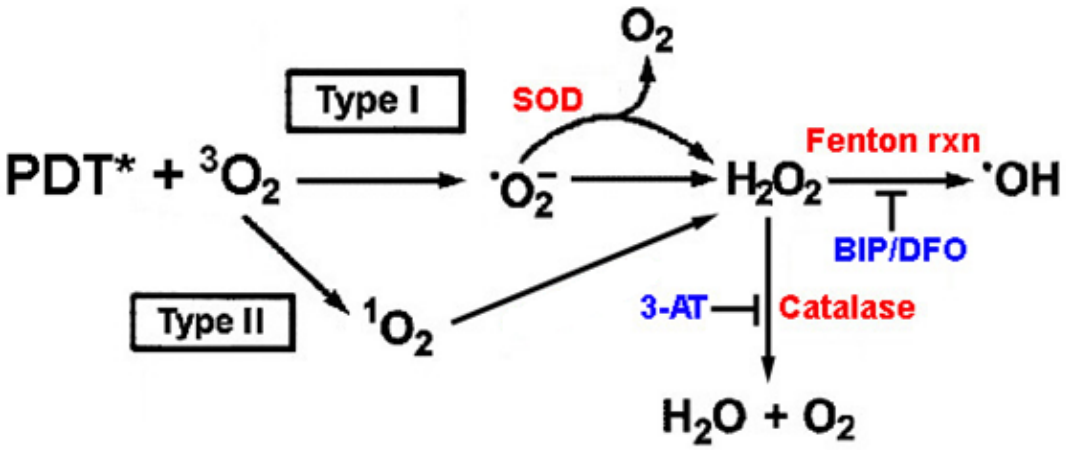

Figure 1.1 Diagram of Type I and II ROS formation during PDT. ROS formation and/or persistence can be altered at several points.

1.3 AIMS

1.3.1 ROS generated by PDT

Many commercially available fluorescent probes are advertised to be specific for the detection of singlet oxygen, superoxide, hydrogen peroxide or other ROS. Specificity of these probes was assessed in experiments involving the different ROS that can be generated during PDT. Effects of peroxidase activity were also examined since this is a common cellular enzyme that can affect ROS formation. During the course of these experiments, a new probe, termed DADB, was reported to be both cell-permeable and specific for singlet oxygen (Oliveira, Severino et al. 2011). Experiments were carried out to evaluate the potential utility of DADB.

1.3.2 A potential role for different ROS in cell death

Singlet oxygen and •OH are sufficiently reactive so that they are expected to oxidize biologic molecules only at the site of formation. Superoxide radical is also likely to be in this class. Hydrogen peroxide, though less reactive, can persist for a much longer time in cells and tissues. Since H_2O_2 can be converted to •OH, inhibition of catalase activity was considered to be a possible means for promotion of PDT efficacy, e.g., by potentiating opportunities for •OH formation. Experiments were designed to evaluate effects of [a] inhibition of catalase activity, and [b] use of an exogenous source of catalase.

1.3.3 Role of oxygenation on PDT efficacy

Tumor hypoxia has proven to be a cause of radiation and chemotherapy resistance. Since oxygen is one of the primary components of PDT, experiments were designed to evaluate the effects of decreasing oxygen levels on the efficacy and photochemical properties of two photosensitizers. As previously mentioned, the photosensitizer NPe6 produces mainly singlet oxygen upon irradiation and localizes in lysosomes. It was later discovered that the photosensitizer termed WST11 also localized in lysosomes (Kessel, Price et al. 2012), but produces only oxygen radicals upon irradiation in an aqueous environment (Ashur, Goldschmidt et al. 2009). This provided us with an opportunity to compare two photosensitizers with the same cellular localization pattern but with markedly different patterns of ROS formation.

CHAPTER 2

USE OF FLUORESCENT PROBES FOR DETECTING ROS AND RNS

2.1 INTRODUCTION

The literature contains numerous reports on the use of fluorescent probes for detection of ROS and reactive nitrogen species (RNS). Invitrogen/Molecular Probes provides a collection of such probes for which the only indication of specificity is provided by the reproduction of a table derived from Setsukinai, Urano et al. (2003). This table compared the fluorescence of two new fluorescein analogs, 3'(*p*-aminophenyl) fluorescein (APF) and 3'(*p*-hydroxyphenyl) fluorescein (HPF), with the fluorescence of 2',7'-dichlorofluorescein (DCF) in a cell-free system containing chemicals that generate different ROS. Experiments were designed to characterize the specificity of some common fluorescent probes.

2.2 MATERIALS AND METHODS

2.2.1 Chemicals and Reagents

Several fluorescent probes including 4',5'-diaminofluorescein (DAF), dihydroethidine (DHE), reduced DCF (H_2DCF-DA) and dihydrorhodamine (DHR), were obtained from Invitrogen/Molecular Probes, Eugene, Oregon. H_2DCF was prepared from the commercially available diacetete by alkaline hydrolysis as described by Doshi, Tian et al. (2007). Diethylamine nitric oxide (DEANO) was provided by the Cayman Chemical Co., Ann Arbor, Michigan. ROS examined were $\bullet O_2^-$ [100 μM KO_2 in anhydrous dimethyl sulfoxide (DMSO)], H_2O_2 (100 μM), and •OH [formed from 20 μM $Fe(NH_4)SO_4$ +100 μM H_2O_2]. Fluorogenic effects of reactive nitrogen species were estimated using DEANO (100 μM). In aqueous media, NO is released from this compound at pH 7. NO is then spontaneously oxidized to the nitrosonium cation.

Horseradish peroxidise (HRP) was purchased from Sigma-Aldrich (St. Louis, MO). The Bcl-2 antagonist HA14-1 was purchased from Ryan Scientific Inc. (Isle of Palms, SC). Benzoporphyrin derivative (Verteporfin, BPD) was purchased from VWR. Stock solutions (10 mM) were prepared in dimethylformamide and stored at 4°C in the dark.

2.2.2 Statistical analyses

Paired one-tailed t-tests were carried out between each group of fluorescent data (± HRP) collected for each probe (Graphpad Software, San Diego, CA). Differences between data sets were scored as statistically significant if $p < 0.05$.

2.2.3 Cell culture

Murine leukemia P388 cells were grown in sealed flasks, using an approximation of Fisher's Medium consisting of αMEM (Sigma-Aldrich, St. Louis, MO) supplemented with $MgCl_2$ (45 mg/L), methionine (75 mg/L), phenylalanine (30 mg/L), valine (30 mg/L), folic acid (9 mg/L), 1 mM glutamine, 1 mM mercaptoethanol, gentamicin, and 10% horse serum. Cells were maintained in suspension culture at 37°C in a 5% CO_2 atmosphere.

2.2.4 Measuring probe fluorescence

Tests were carried out using 5 μM concentrations of each probe in 3 ml of HEPES buffer pH 7.0. Fluorescence was measured 30 min after addition of the reagents specified above. Fluorescence excitation was provided by a 100-W quartz-halogen lamp with the wavelength selected by a monochromator. Fluorescence emission was monitored using an Instaspec IV (Oriel Corp, Stratford, Connecticut) CCD system. Excitation/emission optima were 485 nm/515 nm (DAF), 500 nm/520 nm (DCF), 500 nm/570 nm (DHE), 490 nm/530 nm (DHR), and 490 nm/515 nm (APF). Fluorescence intensity at the emission optimum was recorded. Horseradish peroxidase

(50 μg/ml) was present where specified. In studies involving DHE, DNA (50 μg/ml) was added since the formation of a long-wavelength fluorescence signal depends on binding of the oxidation product(s) to DNA.

All fluorescence measurements are indicated in terms of 'dimensionless' units. These cannot be compared between instruments (fluorescence microscopy, CCD multi-channel signal detection, SLM (steady-state single point fluorescence measurements)). Data obtained from single instruments can, however, be compared.

2.2.5 ROS formation in cell culture

To examine the effects of an RNS detector in vitro, P388 cell suspensions were incubated for 60 min at 37°C with 2 μM BPD + a 5 μM concentration of the RNS probe DAF (added during the final 30 min). The cells were then collected by centrifugation (100 g, 30 s), washed, resuspended in fresh medium at 15°C and irradiated. The light source was a 600 W quartz-halogen lamp with infrared radiation attenuated by a 10 cm layer of water and limited to 690 ± 10 nm by an interference filter (Oriel, Stratford, CT).

2.2.6 Fluorescence microscopy

After irradiation, cells were collected by centrifugation and examined by fluorescence microscopy. Images were acquired with a Photometrics CoolSnap HQ CCD camera operating at −40°C.

2.3 RESULTS AND DISCUSSION

2.3.1 Fluorogenic reactions of ROS probes

Reactions resulting from exposure of five fluorogenic probes to reactive oxygen and nitrogen species were examined in a cell-free system, following procedures reported in Setsukinai, Urano et al. (2003), with minor variations. Results are summarized in Table 2.1. The fluorogenic response by DCF was elicited by •OH >>

H_2O_2 > $\bullet O_2^-$, with enhanced promotion when peroxidase was present. DHE and DHR also responded to these ROS, but no substantial degree of selectivity for any ROS was observed. It has been reported that DHE can be selective for $\bullet O_2^-$ detection if fluorescence (in the presence of DNA) is monitored at 570 nm (Zhao, Kalivendi et al. 2003), but this probe cannot be used for an unambiguous detection of superoxide without an HPLC analysis of products (Zielonka and Kalyanaraman 2010).

The presence of HRP led to a strong promotion of probe fluorescence. HRP can promote probe oxidation by a variety of mechanisms including by direct interactions and via conversion of H_2O_2 to •OH (Kohler and Jenzer 1989; Gorris and Walt 2009). While APF was selective for •OH, especially in the presence of HRP, (Price, Reiners et al. 2009) this probe can also detect $^1O_2$ to a somewhat greater extent than was suggested by Setsukinai, Urano et al. (2003) in the context of PDT. DAF was converted to a fluorescent product by NO > •OH >> H_2O_2 and $\bullet O_2^-$; there was also an increase in fluorescence when HRP was present. It has been reported by Setsukinai, Urano et al. (2003) that APF can readily detect peroxynitrite ion ($ONOO^-$). The lack of response of APF to NO shown in Table 2.1 indicates that this species is not being produced during release of NO from the diethylamine derivative.

Table 2.1 Probe:ROS interactions

	H_2O_2		•OH		$\bullet O_2^-$		NO	
Probe	-HRP	+HRP	-HRP	+HRP	-HRP	+HRP	-HRP	+HRP
DHE	170	1882	3802*	3906*	1372	4241	104	124
DHR	424	6474	3571	12327	51	504	1776§	1726§
H_2DCF	775	2768	10122	23966	427	1806	739	4115
APF	260	1030	5960	6945	42	62	51	210
DAF	226	3288	805	7375	104	1422	2430	5434

Fluorogenic interactions between selected fluorescence probes (5 μM) and reactive oxygen or nitrogen species generated as defined in the text. Numbers represent mean fluorescence emission intensity upon excitation at 490 - 510 nm. Baseline values were subtracted from all determinations. In four replicate determinations, the variation was less than ± 3% of the values shown. The symbols * and § indicate pairs that were not significantly different. [Adapted from the J. Biomed. Opt. 15, 051605, 2010]

2.3.2 HA14-1 and ROS production in cell culture

During a preliminary study, a situation was encountered where a fluorogenic effect involving an ROS probe did not actually detect an ROS. Such interactions really involve only a conversion of a non-fluorescent structure to one that can fluoresce, often as a result of an interaction with an electron donor. The Bcl-2 antagonist HA14-1 was shown to promote the apoptotic response to PDT (Kessel 2008). When a report (Doshi, Tian et al. 2007) appeared indicating that HA14-1 could cause the spontaneous production of ROS, this was considered to be highly unlikely. The ability of HA14-1 to evoke formation of ROS was based on studies involving reduced dichlorofluorescein (H_2DCF). The fluorescence observed when HA14-1 was added to cell cultures was actually derived from a fluorogenic reaction between HA14-1 and serum albumin that exactly mimicked the excitation and emission properties of the oxidized product DCF (Kessel, Price et al. 2008).

2.3.3 Artefacts in the Study of Fluorogenic Interactions

Another potential problem associated with use of fluorescent probes in the context of PDT is illustrated by Figure 2.1. Murine leukemia P388 cells were photosensitized as described in section 2.2.5 and irradiated at 690 nm (90 mJ cm^{-2}), conditions that kill 50% of the cell population. Fluorescence microscopy was then used to assess the resulting fluorogenic interactions using 450–490 nm excitation and monitoring fluorescence at 500–550 or 500–700 nm. Experimental conditions included probe alone [Figure 2.1(a–c)], probe + photosensitizer in the dark [Figure 2.1(d–f)], and after irradiation [Figure 2.1(g–i)].

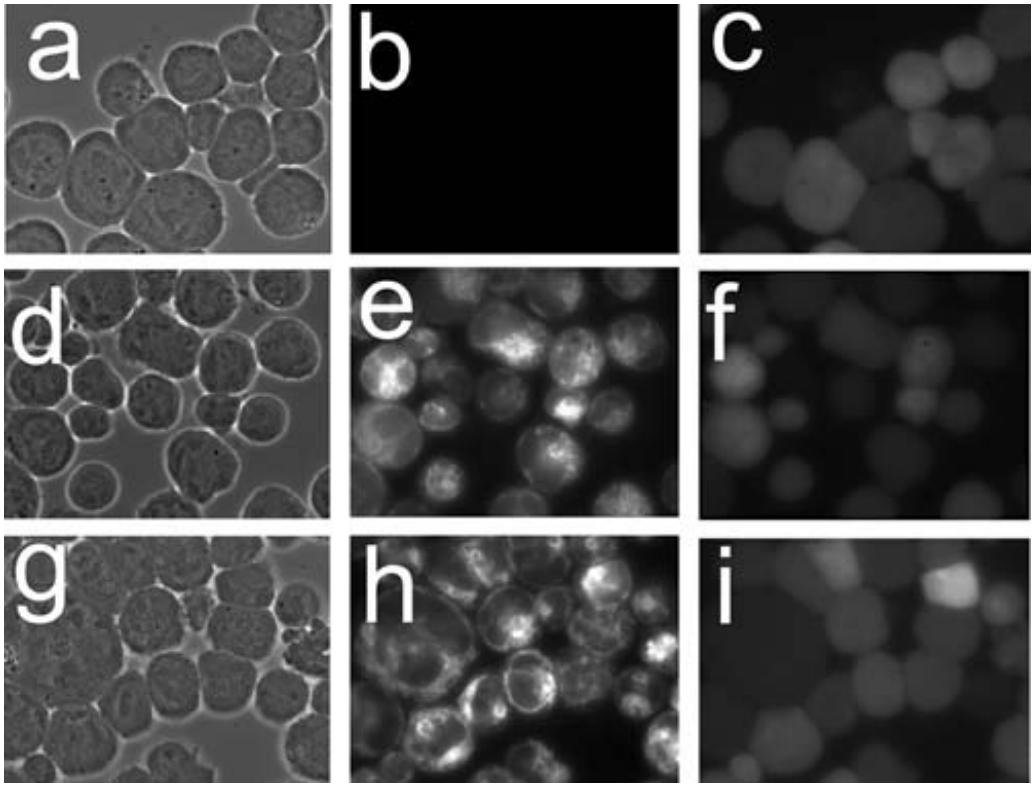

Figure 2.1 Phase contrast and fluorescence images of murine leukemia P388 cells incubated with BPD + DAF and irradiated as described in the text: (a) to (c) control cells containing only DAF, (d) to (f) cells containing DAF + BPD but not irradiated, and (g) to (i) irradiated cells loaded with DAF + BPD. Images (a), (d), and (g) represent phase contrast images; (b), (e), and (h) are fluorescence images acquired at 500–700 nm (BPD and DAF fluorescence) for 100 ms; and (c), (f), and (i) are fluorescence at 500–550 nm acquired for 2000 ms (DAF fluorescence *only*). Photographs are representative of observations for three independent experiments. [Adapted from the J. Biomed. Opt. 15, 051605, 2010]

Images obtained with broadband (500–700 nm) acquisition indicated a substantial fluorogenic response when BPD was present, but this occurred whether or not the photosensitized cells were irradiated [compare 2.1(e) and (h)]. The fluorescence signal was associated with mitochondria, the site where BPD is localized (Peng, Chang et al. 2005). These results remind us that photosensitizing agents also fluoresce, so that care must be taken to exclude their fluorescence from the probe detection. Fluorescence images obtained with narrowband fluorescence acquisition [Figure 2.1(c, f, and i)] revealed the lack of a fluorogenic response to DAF, indicating the

absence of RNS formation upon irradiation. In contrast, broadband fluorescence images do show enhanced fluorescence, but from BPD. The relative intensities of the fluorescence of BPD vs. DAF can be appreciated by noting the time needed for image acquisition: 100 ms for Figure 2.1(b, e, and h) and 2000 ms for Figure 2.1(c, f, and i).

These experiments illustrate potential problems that can occur in studies involving the use of fluorescent probes. There may be fluorogenic interactions not associated with ROS, or confusion between the fluorescence of the probe(s) and of the photosensitizer. In studies reported here, care was taken to eliminate such artefacts.

2.4 CONCLUSIONS

Based on studies in cell-free systems, together with additional experiments that will be reported elsewhere in this document, it appears that DHR can be used to distinguish H_2O_2 from $\bullet O_2^-$, but that peroxidase activity or presence of •OH can complicate interpretation of results. A prior report arrived at a similar conclusion (Henderson and Chappell 1993). DHE is indeed more responsive to $\bullet O_2^-$ than to H_2O_2, but can be oxidized by other ROS (Zielonka and Kalyanaraman 2010). Of the five probes tested, APF was the only product that was highly selective for a single ROS: •OH, and could therefore be responsive to hydrogen peroxide in the presence of peroxidase activity. The pathway to fluorogenic interactions with the probes in the presence of peroxidase activity is not a simple one. The mechanism has been explored by Kobayashi, Nakano et al. (1987). The important point is that variable levels of cellular peroxidase activity can affect the results obtained with many fluorescent probes for ROS.

CHAPTER 3

MONITORING $^1O_2$ AND •OH FORMATION

3.1 INTRODUCTION

The contributions of the various ROS types generated during PDT to the biochemical and morphological changes after PDT are often inferred by the inclusion of ROS type-specific scavengers. What is missing are simple fluorescence-based assays for real-time monitoring of specific types of ROS.

APF and HPF, were synthesized by Setsukinai, Urano et al. (2003) as probes for stable and selective detection of •OH. Both probes were reported to be cell-permeable, relatively insensitive to $•O_2^-$, nitric oxide, and alkyl peroxides and free from the auto-oxidation associated with some other probes. There was some reported responsiveness to $^1O_2$, but only at 0.5% of the level found for •OH. The two probes differed in their responsiveness to hypochlorite ion (ClO^-). APF was converted to a fluorescent form by ClO^- while HPF was not. HPF and APF were examined as cell-permeable probes for the detection of •OH during PDT.

A fluorogenic probe for detection of singlet oxygen described by Flors, Fryer et al. (2006) was also examined. Several relatively specific quenching agents were also employed: these included sodium azide (NaN_3) for $^1O_2$, and DMSO for •OH (Wasil, Halliwell et al. 1987; Wei, Cai et al. 1997).

3.2 MATERIALS AND METHODS

3.2.1 Chemicals and Reagents

For generation of $^1O_2$, TPPS was employed (Porphyrin Products, Logan, UT). Solutions (10 mM) were made up in water and stored at 4°C in the dark. Structures of APF and HPF are shown in Figure 3.1. Singlet oxygen sensor green (SOSG) was

purchased from Invitrogen/Molecular Probes, Eugene, Oregon. Refer to section 2.2.1 for details on other chemicals used in this study.

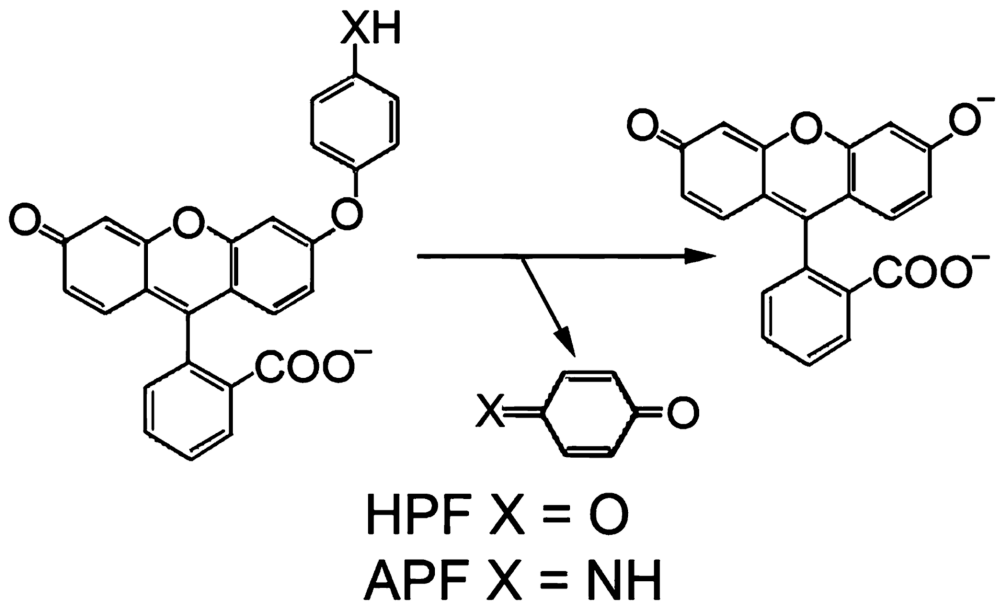

Figure 3.1 Structures of HPF and APF and the oxidative reaction that leads to the formation of fluorescein. [Adapted from Photochem. Photobiol. 85, 1177-81, 2009]

3.2.2 Fluorescence assay procedure

An SLM 48000 fluorometer, modified by ISS (Champaign, IL), was used for acquisition of fluorescence signals as a function of time. When APF or HPF was employed, fluorescence emission at 525 nm was measured upon excitation at 492 nm using 2 nm slit widths for both excitation and emission. With SOSG, the corresponding values were 505 and 525 nm, respectively.

Studies involving a cell-free system were carried out in 1 × 1 × 3 cm glass cuvettes maintained at a temperature of 20°C by a Peltier system, and stirred constantly. When diode lasers were used for irradiation, the influence of stray light from the laser was minimized by insertion of a 500 ± 25 nm interference filter into the emission beam. In all such experiments, the fluorescent probes were present at 3 μM concentrations.

3.2.3 Singlet oxygen formation

Singlet oxygen was generated by a photodynamic reaction in 3 mL of 100 mM phosphate buffer pH 7.0, H_2O or deuterium oxide (D_2O), along with 10 μM TPPS. A 400 μM fiber bundle was used to transfer 649 nm light from a laser diode to the top surface of the cuvette, using a power density of 1 mW cm^{-2}. This permitted the acquisition of a fluorescence signal in real time. Data points were acquired at 4 s intervals over 180 s. The increase in probe fluorescence as a function of time was found to be linear for at least 120 s. Data were collected using Vinci software and the fluorescence intensity values after 120 s were used for analyses.

3.2.4 Formation of hydroxyl radical

This ROS was generated by the Fenton reaction using an initial mixture containing 100 mM phosphate buffer pH 7.0, 0.3 mM $Fe(NH_4)_2(SO_4)_2$, (FAS). Addition of 0.3 mM H_2O_2 resulted in a rapid increase in fluorescence. Data shown represent the steady-state fluorescence signal *minus* the base-line signal obtained before addition of H_2O_2 (Table 3.1). In the data reported and published in Table 3.1, the fluorogenic

Table 3.1 Fluorogenic response to •OH in a cell-free system

	Fluorescence Units	
System	**APF**	**HPF**
H_2O_2	0	
FAS + H_2O_2	6117 ± 420	1339 ± 75
FAS + H_2O_2 + 1% DMSO	170 ± 18*	37 ± 11†
FAS + H_2O_2 + 0.1% DMSO	680 ± 35*	148 ± 36†
FAS + H_2O_2 + 0.02% DMSO	2980 ± 806*	630 ± 25†

Cuvettes contained 3 mL of 100 mM phosphate buffer (pH 7.0), 3 μM APF or HPF and 300 μM FAS plus, where specified, DMSO. After a stable base-line was established (excitation = 492 nm, emission = 525 nm), H_2O_2 was added (300 μM) and the increase in fluorescence was monitored over 120 s, by which time there was no further increase. Data represent the mean ± SD for three determinations (n=3), and represent fluorescence (in arbitrary units) above the base-line level. The symbols * and † represent values that are significantly different from readings obtained with FAS + H_2O_2 ($p < 0.05$). We could not detect a fluorogenic response to hydrogen peroxide alone. [Adapted from Photochem. Photobiol. 85, 1177-81, 2009]

interaction in a sample containing H_2O_2 alone was not evaluated since Setsukinai,

Urano et al. (2003) had reported that this ROS was approximately 0.1% as effective as OH• in inducing APF fluorescence. In a separate study carried out after this table was published, this was confirmed. Using a CCD detection system, we found that the fluorogenic interaction between H_2O_2 and APF negligible; 300 μM H_2O_2 had no effect on the baseline fluorescence intensity of 3 μM APF. An additional 300 μM H_2O_2 added in 100 μM increments had no further effect on APF fluorescence.

3.2.5 Quenching studies

Fluorogenic interactions involving $^1O_2$ and •OH and fluorescent probes were assessed in the absence vs. presence of inhibitors (NaN_3 or DMSO) using SOSG, APF or HPF in systems described above. Data are reported in Figure 3.2 and Figure 3.3 and in Table 3.1.

3.2.6 Cell culture

Cell culture maintenance for L1210 murine leukemia is the same as described in section 2.2.3.

3.2.7 Photodynamic studies in cell culture

L1210 cell suspensions were incubated for 30 min at 37°C with 2 μM BPD + 3 μM APF. See section 2.2.5 for a description of the procedure. In replicate tubes DMSO (1%), 100 μM desferroxamine (DFO) or both reagents were added. The light dose was 67.5 mJ cm^{-2} at 690 ± 5 nm, as determined with a ScienTech H10T radiometer. This PDT dose was found to reduce cell viability to 11 ± 3% of control values, as indicated in prior studies involving clonogenic assays.

3.2.8 Fluorescence microscopy

After irradiation, cells were collected by centrifugation and examined by fluorescence microscopy using 450–490 nm excitation, monitoring emission at 520–600

nm. The images were acquired by a Photometrics CoolSnap HQ CCD camera operated at −40°C. An exposure time of 1000 ms was required to obtain the images shown in Figure 3.4. A B2A filter cube was used (excitation = 450–490 nm). The emission was controlled by a high-pass 520 nm filter and an additional 600 nm low-pass filter to screen out fluorescence derived from BPD. Images of cellular fluorescence were captured using MetaMorph software (Molecular Devices, MDS Analytical Technologies). Average pixel intensities were determined using 'region statistics' procedure.

3.2.9 Region statistics analysis procedure

A 'thresholding' process was used to select only those portions of the image representing cellular fluorescence. The black pixels in the background were gated (not counted) and omitted from the calculations. Any extremely bright pixels were also gated and an average grayscale analysis was then calculated as the summation of the values for each pixel contained in the images of the cells (0 = black, 255 = white). This value was then divided by the total number of pixels to provide an average pixel brightness.

3.2.10 Statistical analyses

Data for fluorescent probes were analyzed by using paired one-tailed t-tests. Differences between data sets were scored as statistically significant if $p < 0.05$. Statistical analyses of 'region statistics' data was done using unpaired one-tailed t-tests, using the number of cells in the field as the sample size, n. Differences between data sets were scored as statistically significant if $p < 0.05$.

3.3 RESULTS AND DISCUSSION

3.3.1 Fluorogenic response of HPF and APF to •OH and quenchers

The effects of •OH on APF and HPF fluorescence are summarized in Table 3.1.

APF yielded ~5-fold more fluorescence during •OH formation than did HPF. Setsukinai, Urano et al. (2003) reported that APF was more sensitive than HPF to oxidation by •OH by a factor of 1.7. In experiments reported here, FAS replaced the salt $Fe(ClO_4)_2$ employed by Setsukinai, Urano et al. (2003). Use of the latter resulted in formation of a precipitate in phosphate buffer. There was no precipitation when FAS was used as the source of ferrous iron.

In a cell-free system, the fluorogenic reaction of •OH with HPF or APF was quenched ~50% by 0.02% DMSO (vol / vol). A concentration of 0.1% DMSO, often said to be safe for use in biological studies, was found to decrease the fluorogenic response of APF to •OH by >90% (Table 3.1). For both APF and HPF, additions of DMSO at all concentrations led to significant decreases in fluorescence intensities from the baseline reading with FAS + H_2O_2.

3.3.2 Determinants of singlet oxygen formation

Singlet oxygen formation was monitored with the probe SOSG (Figure 3.2, top). During irradiation of an aqueous solution of TPPS + SOSG, there was an increase in 525 nm fluorescence that was markedly enhanced when D_2O was substituted for water. This effect is to be expected since the lifetime of the triplet state is strongly promoted in deuterated solvents (Moan and Wold 1979; Gorman and Rogers 1989). The fluorogenic effect of $^1O_2$ on SOSG was very slightly enhanced by the presence of 100 mM phosphate buffer pH 7.0, compared with water alone.

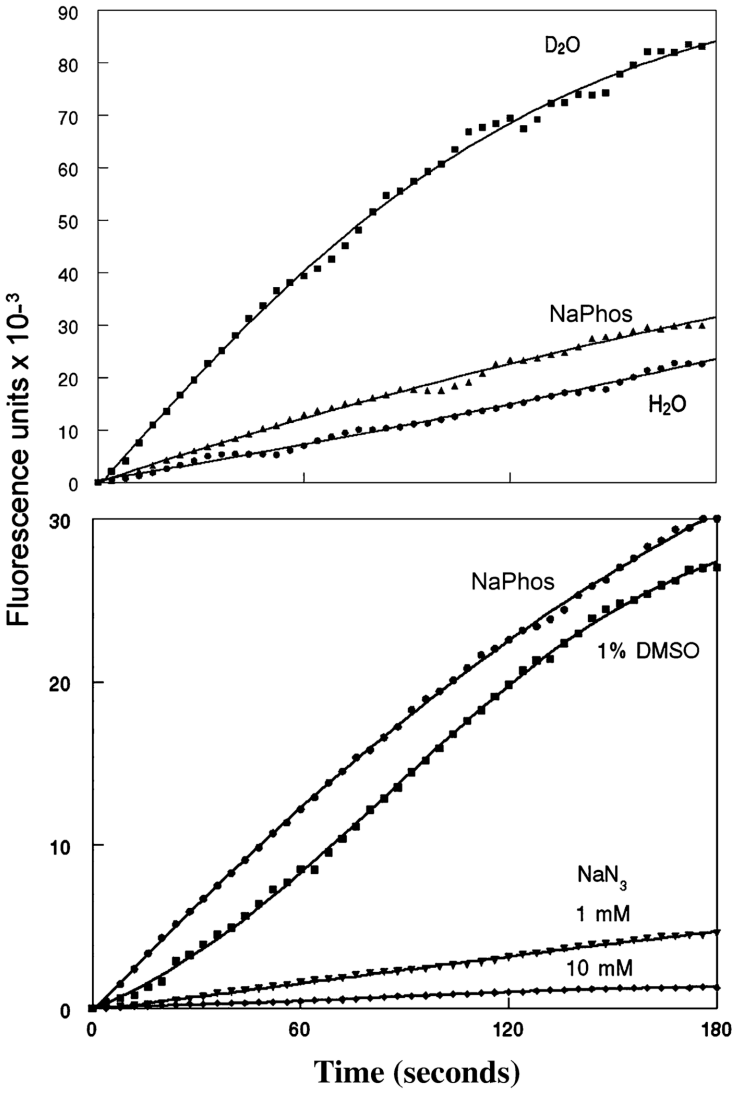

Figure 3.2 Monitoring singlet oxygen formation with SOSG. Top: fluorogenic interaction between 3 μM SOSG and $^1O_2$ during the irradiation (649 nm) in 10 μM TPPS. Solvents were D_2O, 100 mM sodium phosphate buffer pH 7.0, or water, using a light flux of 1 mW cm^{-2}. Fluorescence was monitored using excitation = 505 nm, emission = 525 nm. Bottom: fluorescence quenching during irradiation of SOSG + TPPS in phosphate buffer by 1 or 10 mM NaN_3 and by 1% DMSO. Similar results were obtained with an additional two replicate experiments. [Adapted from Photochem. Photobiol. 85, 1177-81, 2009]

Quenching studies carried out with SOSG in phosphate buffer (Figure 3.2, bottom) showed only a minor effect of 1% (vol / vol) DMSO on $^1O_2$-mediated fluorescence, but a substantial quenching of the fluorogenic reaction by NaN_3.

3.3.3 Fluorogenic responses of HPF and APF to singlet oxygen

Irradiation of an aqueous solution containing APF + TPPS resulted in a fluorogenic response that was enhanced >25-fold in D_2O (Figure 3.3). This fluorogenic reaction was also slightly greater in phosphate buffer than in water. Additional studies (in phosphate buffer) revealed only a slight quenching of APF fluorescence by 1%

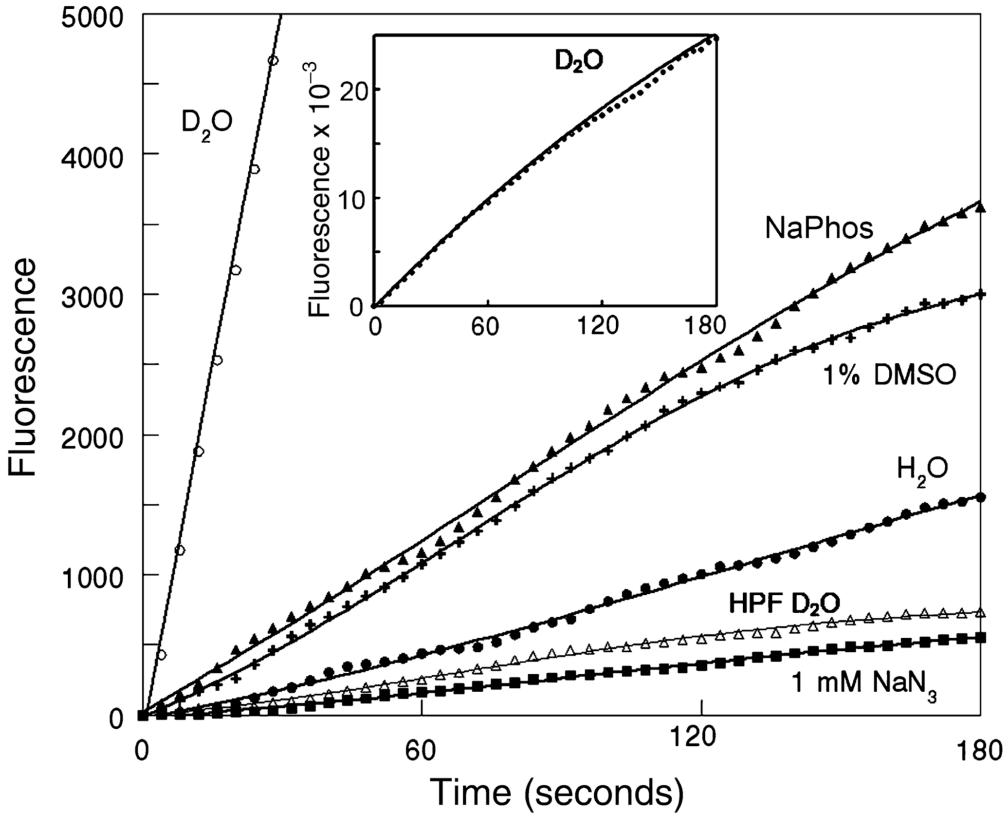

Figure 3.3 Fluorogenic responses of APF and HPF to singlet oxygen using 10 μM TPPS + APF in D_2O, phosphate buffer or water during irradiation (649 nm). Also shown are effects of 1 mM NaN_3 and 1% DMSO in phosphate buffer. For comparison, the fluorogenic reaction with HPF in D_2O is also shown. Inset: the fluorogenic effect during irradiation of TPPS + APF during 180 s in D_2O. For all studies, excitation = 492 nm, emission = 525 nm. Similar results were obtained with an additional two replicate experiments. [Adapted from Photochem. Photobiol. 85, 1177-81, 2009]

DMSO, but a very substantial decrease by 1 mM NaN_3 (Figure 3.3). These characteristics are consistent with the behaviour of $^1O_2$ + SOSG shown in Figure 3.2.

HPF was substantially less sensitive to a fluorogenic reaction with $^1O_2$ than was APF. In D_2O, the production of fluorescence upon the interaction of $^1O_2$ with APF during irradiation proceeded at a ~35-fold greater rate than with HPF (Figure 3.3, line designated "HPF D_2O"). These values differ from what was reported in Setsukinai, Urano et al. (2003), where HPF was found to be ~50% as responsive to $^1O_2$ as APF. In Setsukinai, Urano et al. (2003), the comparison was also carried out in phosphate

buffer. Deuterium oxide was used to increase the signal-to-noise ratio since the fluorogenic interaction between HPF and $^1O_2$ in H_2O or phosphate buffer was barely detectable (not shown). Since DMSO is known to quench •OH but not $^1O_2$ (Wasil, Halliwell et al. 1987; Wei, Cai et al. 1997), these data show that both APF and HPF can detect $^1O_2$ formed during PDT.

It was concluded that APF can detect the high concentration of singlet oxygen formed during PDT involving this photosensitizing agent, even though APF is relatively insensitive to singlet oxygen. In later studies, a much more sensitive singlet oxygen probe was employed: DADB.

3.3.4 ROS detection in cell culture

TPPS was useful for studies in an aqueous cell-free system since it does not aggregate in aqueous solution. Aggregation can result in a significant reduction in ROS formation upon irradiation. In order to carry out studies in cell culture, a more hydrophobic agent was used: BPD. This photosensitizer was much more readily accumulated by L1210 cells. To determine the potential usefulness of APF in PDT studies, we incubated L1210 cells with APF and BPD, followed by irradiation to achieve an LD_{90} PDT dose. Fluorescence images (Figure 3.4) were obtained at the same camera settings. A 600 nm low-pass filter was placed in the emission pathway to eliminate fluorescence derived from the photosensitizing agent. In non-irradiated cultures, only a weak APF fluorescence could be detected (Figure 3.4, panel A).

Irradiation of photosensitized cells resulted in substantial fluorescence derived from APF (Figure 3.4, panel B). Addition of 1% DMSO or the iron-chelator DFO resulted in a decrease in this fluorescence (Figure 3.4, panels C and D). Adding both reagents simultaneously did not significantly increase this quenching (Figure 3.4, panel

E). A 'region statistics' analysis is summarized in Table 3.2. Images were subjected to a 'threshold' analysis where the black pixels were gated (not counted). Any extremely bright pixels were also eliminated and an analyses of the average pixel brightness is then produced.

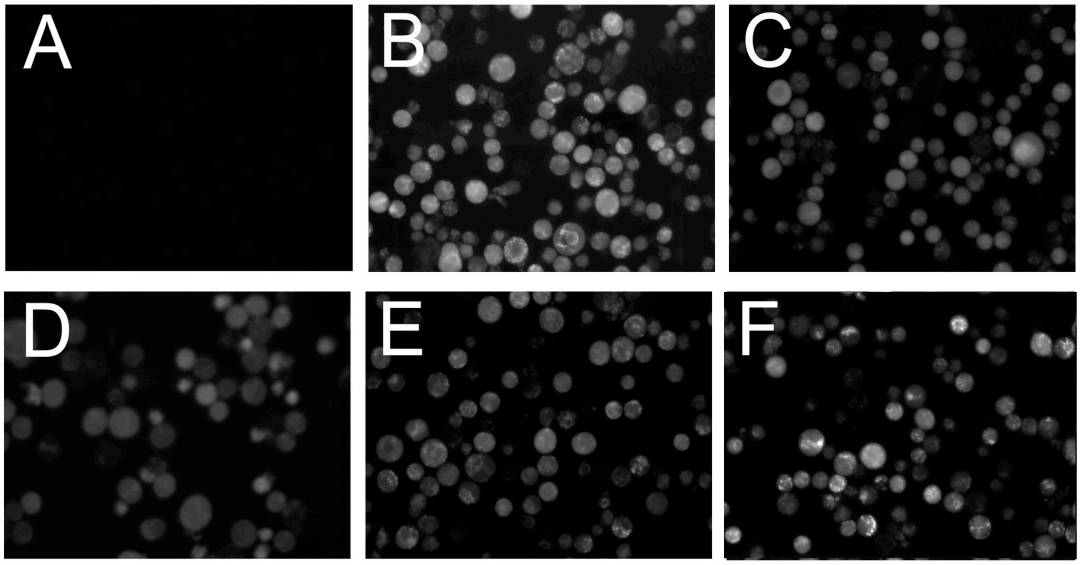

Figure 3.4 Fluorescence images of APF fluorescence using L1210 cells photosensitized by BPD. A = dark control (no irradiation), B–E = irradiated cells, B = no additions, C = 1% DMSO, D = 100 μM DFO, E = 1% DMSO + 100 μM DFO, F = 0.1% DMSO. Inhibitors were present during BPD loading, and added to the culture medium during irradiation. Photographs are representative of observations for three independent experiments. [Adapted from Photochem. Photobiol. 85, 1177-81, 2009]

Table 3.2 Region statistics analysis

Conditions	Average grayscale value
Control	3.8 ± 4.4
BPD	58.5 ± 16.35
BPD + 1% DMSO	32.8 ± 10.3*
BPD + 100 μM DFO	32.45 ± 5.8*
BPD + both	28.7 ± 14.5*
BPD + 0.1% DMSO	49 ± 12.7

These numbers represent the pixel brightness analyses (mean ± SD) of images shown in Figure 3.4. *These numbers are statistically different from treatment with BPD ($p < 0.05$). [Adapted from Photochem. Photobiol. 85, 1177-81, 2009]

DFO is known to quench hydroxyl radical formation generated via the Fenton reaction (Hoe, Rowley et al. 1982; Entman, Youker et al. 1992; Faurschou and

Gniadecki 2008). Analysis of intensities indicates that ~50% of the total APF fluorescence was derived from processes quenched equally by DFO or DMSO, presumably representing •OH (Table 3.2). Adding both reagents did not further promote fluorescence quenching, consistent with the supposition that the fluorescence diminished by DMSO represents •OH. Incubation of the cell culture with as little as 0.1% DMSO was also found to quench the fluorescence of •OH derived APF fluorescence after irradiation.

Experiments were designed to determine whether HPF might be useful for monitoring •OH formation during irradiation of photosensitized cells. The interaction between •OH and HPF produces only 20% of the fluorescence intensity observed with APF (Table 3.1). As a result, detection of a fluorescent signal from HPF after an LD_{90} PDT dose would require a 5000 ms exposure. This was associated with substantial photobleaching of the probe (not shown). Since SOSG cannot be used with intact cells because of its inability to penetrate the cell membrane (Setsukinai, Urano et al. 2003) and the often-used probe DCF is readily auto-oxidized (Setsukinai, Urano et al. 2003), it was considered that APF or HPF might be useful for "on-line" monitoring of $^1O_2$ formation, in the presence of DMSO to suppress •OH formation. A better procedure for assessing singlet oxygen formation, involving a new probe (DADB) was later developed.

3.4 CONCLUSIONS

These studies show that in the context of PDT where a very substantial concentration of $^1O_2$ is formed, APF can detect this ROS and might be a useful probe for this purpose if DMSO is used to suppress •OH formation. But this represents a 'less than ideal' situation and better singlet oxygen probes are clearly needed.

APF and HPF can be used as probes for the detection of •OH and hypochlorite

(Franco, Panayiotidis et al. 2007; Indo, Davidson et al. 2007; Sumitomo, Shishido et al. 2007). It was initially reported that these probes were relatively insensitive to $^1O_2$ (Setsukinai, Urano et al. 2003). However, studies indicate that, under conditions associated with PDT, where high levels of singlet oxygen can be formed, fluorogenic interactions with $^1O_2$ can be significant, with APF substantially more sensitive to $^1O_2$ than HPF.

Quenching studies, carried out in a cell-free system, indicated that 1.0% DMSO could suppress >90% of the APF fluorescence derived from •OH (Table 3.1) without affecting the signal derived from $^1O_2$ (Figure 3.3). The ability of concentrations of DMSO as low as 0.02% (not shown) to partially quench •OH, in a cell-free system, means that use of this agent should be minimized in any study designed to assess formation or effects of this ROS. This sensitivity to DMSO was, however, reduced in studies carried out with intact cells (Figure 3.4). A study with murine leukemia L1210 cells and the photosensitizing agent BPD revealed that the use of APF in the presence vs. absence of DMSO might be a feasible approach for monitoring •OH formation during irradiation of photosensitized cells (Figure 3.4) but is clearly not ideal. In the presence of DMSO, APF could be used to assess $^1O_2$ formation during PDT, but, as is reported below, a better option involving the probe DADB was later developed.

It has been proposed (Chekulayeva, Shevchuk et al. 2006) that the conversion of 2-deoxy-D-ribose to products that react with thiobarbituric acid could be an additional test for •OH formation during PDT, as could a fluorescence assay involving derivatives of terephthalate (Saran and Summer 1999). While these could be useful probes for assessing •OH formation during PDT, they would need to be evaluated for possible interactions with $^1O_2$.

CHAPTER 4

A ROLE FOR HYDROGEN PEROXIDE IN THE EFFICACY OF PHOTODYNAMIC THERAPY

4.1 INTRODUCTION

Promotion of PDT efficacy should lead to enhanced tumor eradication. This can be useful, *e.g.* if light penetration is impaired or the concentration of the photosensitizer is suboptimal. The anti-apoptotic protein Bcl-2 is a known target for PDT, and adding Bcl-2 antagonists can promote photokilling at low PDT doses (Kessel 2008). PDT can also lead to enhanced autophagy, a survival process that can offer protection from photodamage, resulting in a "shoulder" on the dose–response curve (Kessel and Arroyo 2007). In this study, the role of H_2O_2 formed during PDT was examined as a factor in the phototoxic response. These studies were carried out in P388 murine leukemia cells, using BPD as the photosensitizing agent. BPD is known to catalyze an apoptotic response (Granville, Levy et al. 1997) to PDT. During the photodynamic process, a variety of ROS are produced, including $^1O_2$, H_2O_2 and •OH (Girotti 1998).

Two procedures were used to modulate intracellular H_2O_2 levels during irradiation of photosensitized cells. Both involved altering the level of intracellular catalase activity. This enzyme is involved in the predominant detoxification pathway for H_2O_2, catalyzing its conversion to $H_2O + O_2$. Catalase activity can be inhibited by the irreversible antagonist 3-amino-1,2,4-triazole (3-AT). An exogenous cell-permeable catalase derivative was also used to enhance H_2O_2 degradation: the enzyme analog termed CAT_{SKL} efficiently traffics to the peroxisome, where catalase activity normally resides (Terlecky, Koepke et al. 2006; Koepke, Nakrieko et al. 2007; Terlecky and Koepke 2007). Analysis of the intracellular H_2O_2 concentration was provided by the fluorescent

probe DHR (Crow 1997; Qin, Lu et al. 2008), a product that is converted to a fluorescent analog upon oxidation by H_2O_2. Other analytical procedures were used to monitor catalase concentrations and activity, phototoxicity and apoptosis, a common death mode after PDT. A reaction between H_2O_2 and ferrous iron results in the formation of the highly reactive hydroxyl radical. This reaction was first described by Fenton (Fenton 1984):

$$Fe^{+2} + H_2O_2 \rightarrow Fe^{+3} + OH^- + \bullet OH$$

To decrease the conversion of H_2O_2 to •OH, 2,2′-bipyridyl (BIP) was used to chelate Fe^{+2} (Breuer, Epsztejn et al. 1995) and thereby antagonize the Fenton reaction.

4.2 MATERIALS AND METHODS

4.2.1 Chemicals and Reagents

Refer to section 2.2.1 for any chemicals and reagents used in this study. Amino acids, tissue culture media and chemicals were purchased from Sigma-Aldrich (St. Louis, MO); sterile horse serum was provided by Atlanta Biologicals (Laurenceville, GA); DEVD-R110 by Molecular Probes (Invitrogen; Eugene, OR). Terlecky's group has developed a modified catalase preparation (CAT_{SKL}) that can serve as an endogenous source of catalase (Terlecky, Koepke et al. 2006; Terlecky and Koepke 2007). CAT_{SKL} was engineered to contain both a cell penetrating peptide (CPP) to allow the enzyme to be rapidly endocytosed into cells, and a peroxisomal targeting signal (PTS), that targets the catalase directly to the peroxisomal membrane.

4.2.2 Cell culture

See section 2.2.2 for details on P388 cell culture maintenance.

4.2.3 Photodynamic studies in cell culture

Photosensitization of cell cultures was previously described in section 2.2.5. CAT_{SKL} or 3-AT was present during the loading incubation when specified.

4.2.4 Survival measurements

Clonogenic assays were used to determine PDT efficacy. P388 cells were photosensitized as described in section 2.2.5, then irradiated (20–200 mJ cm^{-2}). Cell dilutions containing approximately 300 cells per 60 mm^2 dishes (as determined with a Coulter Cell Counter) were plated on soft agar in triplicate. After a 7- to 9-day growth interval, colonies were counted and their numbers compared with untreated controls. The plating efficiency of control (untreated) cell cultures was ~70%.

4.2.5 BPD transport

Cells were incubated with a 2 μM concentration of BPD for 30 min at 37°C, then collected by centrifugation. Samples of supernatant fluid and the entire cell pellet were dispersed in a non-ionic detergent Triton X-100 (10 mM) and the resulting fluorescence (695–700 nm) was measured upon excitation at 400 nm. The distribution ratio could then be determined. The distribution ratio represents the ratio of [BPD concentration/mg cells]/[BPD concentration/μl media]. Effects of concurrent treatment with 3-AT, BIP or CAT_{SKL} were also assessed.

4.2.6 BPD localization

Cells were examined by fluorescence microscopy after incubation with 2 μM BPD for 30 min at 37°C (400 ± 20 nm excitation, measuring fluorescence at wavelengths >650 nm. Where specified, 3-AT (30 mM) or CAT_{SKL} (1000 U) was also present.

4.2.7 Fluorescence microscopy

Fluorescence images were acquired using a Nikon Eclipse E600 microscope and

a CoolSnap HQ CCD camera (Photometrics, Tucson, AZ). Images were subsequently processed using MetaMorph software. For photographs shown in Figure 4.2, a stack of 20 images was acquired using a Prior ProScan Z-drive. These were subject to 3-D deconvolution using AutoQuant Deblur software (Media Cybernetics Inc., Bethesda, MD).

4.2.8 Chromatin labelling

To assess apoptotic chromatin in cell nuclei, P388 cells were incubated with 1 μM HO33342 (HO342) for 5 min at 37°C, washed once and examined by fluorescence microscopy using 360–390 nm excitation; 400–450 nm emission.

4.2.9 Fluorimetric detection of H_2O_2 in cell culture

P388 cell suspensions (2×10^6 cells mL^{-1}) were incubated for 30 min at 37°C with 2 μM BPD + 5 μM DHR along with (as specified) 3-AT (30 mM), 1000 U of pure recombinant CAT_{SKL} (provided as a solution containing 148,000 U mg^{-1} protein) or 2 μM BIP. The cells were then resuspended in fresh medium, adding back 3-AT, CAT_{SKL} or BIP if initially present. The cells were irradiated at 15°C (690 ± 10 nm, 100 mJ cm^{-2}). Fluorescence of the DHR oxidation product was measured using a multi-channel analyzer using 490 nm excitation and recording fluorescence at 525 nm. Fluorescence intensity of DHR alone was < 100 units for all dark controls.

The fluorogenic interaction between H_2O_2 and DHR could also be measured in real time during irradiation using an SLM 48000 series fluorometer. Cell cultures were prepared as outlined above, then resuspended in 3 mL of fresh medium in 1 × 1 × 3 cm glass cuvettes. The temperature was maintained at 20°C by a Peltier system and the contents stirred. Irradiation was carried out using light from a 690 nm diode laser (1 mW cm^{-2}) directed at the top surface of the cuvette via a 400 μ fiber, using a GRIN (graded-

index) lens to focus the beam to a 0.9 cm diameter circle. Fluorescence emission from oxidized DHR (525 nm) was monitored using 490 mn excitation. The “slow kinetic” mode was used for data acquisition with points collected every 4 s for 180 s. Influence of 690 nm irradiation on the emission photomultiplier detector was eliminated by insertion of a 550 nm low-pass filter into the emission beam.

4.2.10 DEVDase assays

Cells were incubated as outlined above, irradiated as specified, then lysed in 100 µL of buffer containing 50 mM Tris pH 7.2, 0.03% Nonidet P-40 and 1 mM DTT. The lysates were briefly sonicated and debris removed by centrifugation (10,000 g for 1 min). The supernatant fluid (50 µL) was mixed with 40 µM DEVD-R110, 10 mM HEPES pH 7.5, 50 mM NaCl and 2.5 mM DTT in a total volume of 100 µL. The rate of increased fluorescence emission, resulting from the release of rhodamine-110 from the fluorogenic substrate (Cai, Zhang et al. 2001), was measured over 30 min at room temperature using a Fluoroskan Ascent fluorescent plate reader. DEVDase activity is reported in terms of nmol product $min^{-1}mg^{-1}$ protein. Control determinations were made on extracts of untreated cells. Each assay was performed in triplicate. The Lowry method was then used to determine protein concentrations.

4.2.11 Catalase activity

Catalase activity was monitored by spectrophotometry. Activity is defined in terms of conversion of H_2O_2 to $H_2O + O_2$; this results in the loss of H_2O_2 absorbance at 240 nM. One unit of catalase is defined as the amount needed to convert 1.0 mol of H_2O_2 to $O_2 + H_2O$ per minute at pH 7.0 and 23°C. In initial studies, cell extracts (40 µL) were added to quartz cuvettes containing 3 mL of 50 mM phosphate buffer pH 7.0 and 20 mM H_2O_2. The initial optical density was ~0.5. Loss of absorbance was then

determined over 30 s intervals. Since precise timing of short intervals can be inaccurate, loss of H_2O_2 was more accurately determined by a colorimetric assay involving a product formed from peroxide and acidified titanium sulfate (Fujimoto 1965; Storrie and Madden 1990). After incubating a mixture of H_2O_2 + cell lysate for 30 min at room temperature, a solution of $TiOSO_4$ in 1 N H_2SO_4 is then added, with the optical density at 405 nm measured 15 min later.

4.2.12 Western blot analyses

Conversion of procaspase-3 to the active form, along with the ability of CAT_{SKL} to enhance the catalase level in P388 cells was assessed via Western blots of whole cell lysates. After specific treatments, P388 cell cultures were lysed in BD BaculoGold™ Insect Cell Lysis Buffer (BD Biosciences, San Jose, CA). The samples were then centrifuge at 10,000 g for 1 min to remove any debris and the Lowry method was used to determine the protein concentration of the samples. The lysates were diluted with SDS-PAGE buffer adjusting for protein concentration, and heated to 85°C for 5 min. Aliquots containing 40 g of protein were subjected to electrophoresis on 4–20% tris-glycine gels (life Technologies, Carlsbad, CA) and the proteins transferred to polyvinylidene fluoride membranes. Nonspecific antibody binding was blocked by incubating the membranes in 5% membrane blocking agent in TBS-T for one hour on a rotator at room temperature. The membranes were washed three times for five minutes each with TBS-T and then incubated with the primary antibodies for one hour. Anti-mouse/human antibodies to caspase-3 and catalase were obtained from BD Pharmingen (San Jose, CA). After incubation with the primary antibodies, the membranes were subsequently washed again, followed by one-hour incubation with an alkaline phosphatase-linked secondary antibody at room temperature (Amersham ECF

Western Blotting Reagent Kit, GE Healthcare, UK). A proprietary substrate is then cleaved by phosphatase activity to form a fluorescent product that could be detected with the using a Storm imaging system (Molecular Dynamics) and quantified using the ImageJ analysis program. Actin analysis was carried out to insure equal loading of proteins.

4.2.13 Statistical Analyses

A paired one-tailed t-test was used to analyze data shown in Table 4.1. This method was also used to analyze apoptotic nuclei in Figure 4.3.

4.3 RESULTS AND DISCUSSION

4.3.1 PDT dose–response information

The effect of varying the light dose on BPD-induced phototoxicity, assessed by clonogenic studies, is shown in Figure 4.1. This demonstrates the fairly steep dose–response curve typical of PDT. A 50% loss of viability occurred at a light dose of ~60 mJ cm^{-2}. Effects of selected additions are shown in Table 4.1 and described in section 4.3.5.

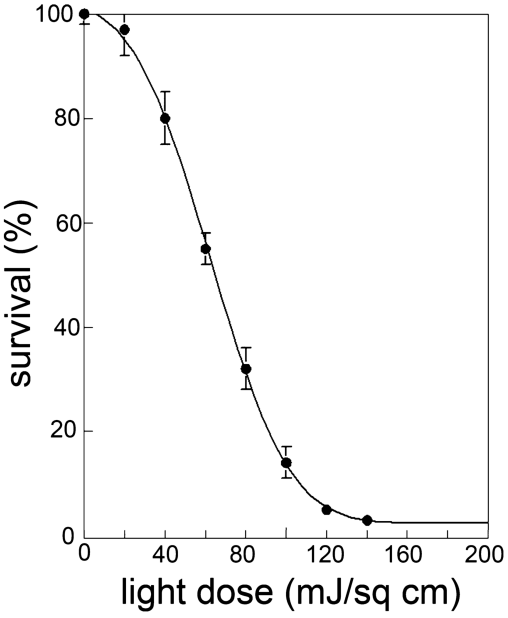

Figure 4.1 P388 cells were photosensitized with BPD (2 μM) and irradiated at varying light doses. Viability was determined by clonogenic assays. Similar results were observed in a second independent experiment. [Adapted from Photochem. Photobiol. 85, 1491-6, 2009]

4.3.2 BPD transport

Incubation of cells with a 2 μM concentration of the photosensitizer BPD resulted in a drug distribution ratio of 21.4 ± 1.5. This was not affected by the presence of 3-AT, BIP or CAT_{SKL} at concentrations specified in the legend to Table 4.1.

4.3.3 BPD localization

The pattern of BPD localization suggests affinity for mitochondria >> ER. This is consistent with data shown previously (Runnels, Chen et al. 1999). This pattern was not altered when cells were incubated with BPD + 3-AT or CAT_{SKL} (Figure 4.2) or BIP (data not shown).

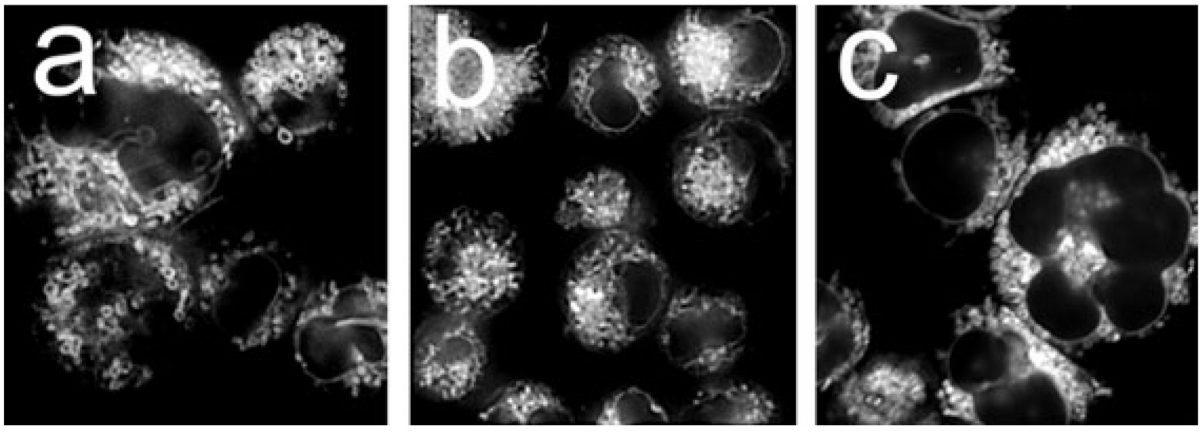

Figure 4.2 Fluorescence microscopy demonstrating the localization of BPD in P388 cells. Cells were incubated with a 2 μM concentration of the sensitizer for 30 min at 37°C and images acquired as described in the text. a = BPD alone; b = BPD + 30 mM 3-AT; c = BPD + 1000 U CAT_{SKL}. Photographs are representative of observations for three independent experiments. [Adapted from Photochem. Photobiol. 85, 1491-6, 2009]

4.3.4 Effects of 3-AT and CAT_{SKL} in the dark

While 3-AT and CAT_{SKL} had significant effects on catalase activity in control cells, neither induced activation of DEVDase. A significant change in levels of H_2O_2 was not detected in cells kept in the dark with these agents as well (Table 4.1, columns 2–4), as shown by the absence of significant DHR oxidation to a fluorescent product.

4.3.5 Catalase modulation and PDT-induced effects

An LD_{90} PDT dose resulted in a significant degree of DEVDase activation 30 min after irradiation of photosensitized cells. This was enhanced by 3-AT and impaired with CAT_{SKL}. The overall level of catalase activity was not significantly altered by PDT. The presence of the ferrous iron-chelating agent BIP resulted in a decrease in the level of DEVDase activity and in the LD_{50} light dose, suggesting a phototoxic effect of •OH, derived from H_2O_2, thereby enhancing the pro-apoptotic effect of PDT (Table 4.1). In agreement with the DEVDase data (Table 4.1), addition of CAT_{SKL} decreased numbers of apoptotic nuclei 60 min after irradiation, while addition of 3-AT had the opposite effect (Figure 4.3). Numbers of apoptotic nuclei determined in three such fields indicated >1% in untreated cells, 58 ± 4% in cultures after PDT, 31 ± 5% in cells treated with PDT in the presence of CAT_{SKL} and 88 ± 3% in cells treated with PDT + 3-AT. Incubation with these agents offered a significant degree of protection (CAT_{SKL}) or promotion (3-AT) of phototoxicity as determined by paired one-tailed t-tests ($p < 0.05$).

Table 4.1 Effects of CATSKL and 3-AT on PDT efficacy

	Controls*			**Irradiated cells†**			
Assay		+ 3-AT	+ CAT_{SKL}		+ 3-AT	+ CAT_{SKL}	+ BIP
DEVDase	0.3 ± 0.1‡	0.4 ± 0.07	0.3 ± 0.09	5.1 ± 1.2	7.6 ± 1.3	3.9 ± 1.3	4.5 ± 0.9
Catalase	6.23 ± 0.42§	0.93 ± 0.12	26.2 ± 1.3	6.12 ± 0.62	0.99 ± 0.17	24.4 ± 0.84	5.8 ± 0.4
DHR	< 100‖	< 100	< 100	953 ± 25	2053 ± 41	356 ± 14	901 ± 34
LD_{50}				61 ± 3¶	47 ± 2	72 ± 3	66 ± 4

Effects of CAT_{SKL} and 3-AT on PDT efficacy. Data represent the mean ± SD for three independent experiments. * Cells were incubated for 30 min with no additions or in the presence of 30 mM 3-AT or 1000 U of CAT_{SKL}; † Cells were incubated with 2 μM BPD plus specified additions (30 mM 3-AT, 1000 U of CAT_{SKL} or 2 μM BIP) for 30 min, then irradiated using an LD_{90} PDT dose; ‡ nmol product min^{-1} mg^{-1} protein; § μmol H_2O_2 metabolized $min^{-1}mg^{-1}$ protein; ‖ Relative fluorescence; ¶ Light dose (mJ cm^{-2}) required for a 50% decrease in viability. [Adapted from Photochem. Photobiol. 85, 1491-6, 2009]

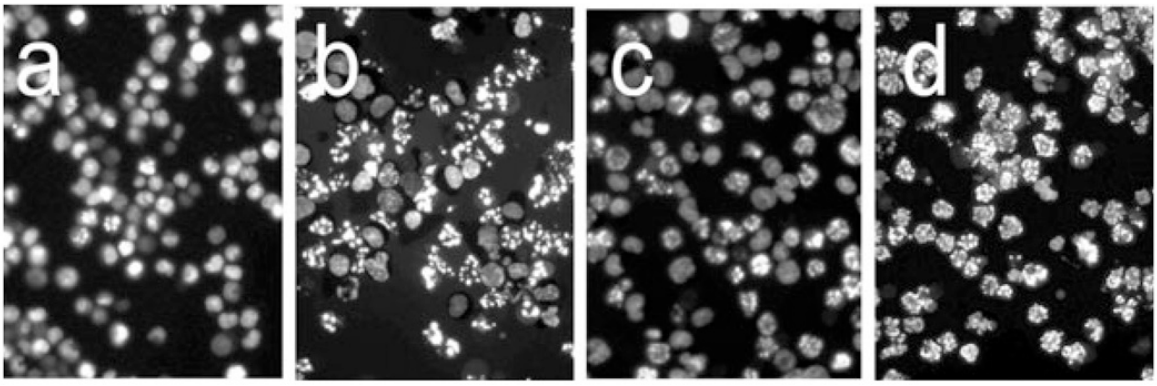

Figure 4.3 Effects of PDT on P388 chromatin as indicated by HO342 labelling using fluorescence microscopy. a = control (untreated) cells; b–d = cells 60 min after receiving an LD_{90} PDT dose; c = 1000 U of CAT_{SKL} present; d = 30 mM 3-AT added as specified in the text. Photographs are representative of observations for three independent experiments. [Adapted from Photochem. Photobiol. 85, 1491-6, 2009]

An increase in DEVDase activity is expected to be accompanied by conversion of procaspase-3 to the active form. Western blot analysis of (Figure 4.4) confirmed this assumption. Using LD_{50} and LD_{90} PDT doses, it was determined that 3-AT increased the conversion of procaspase-3 (32 kDa) to the active form (17 kDa). ImageJ analysis of the caspases-3 bands showed that the intensity was >2 fold greater when 3-AT was present during the irradiation step (Table 4.2).

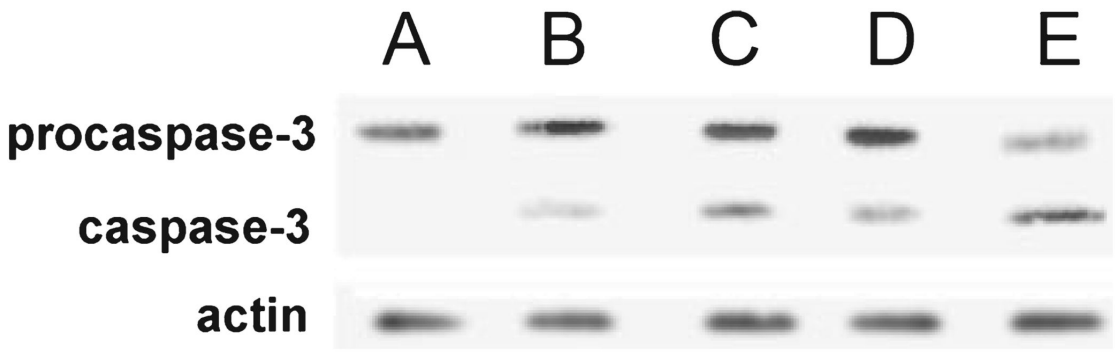

Figure 4.4 Activation of procaspase-3. Extracts were prepared 30 min after irradiation. A, controls (dark); B–E, cells treated with 2 μM BPD and irradiated (60 mJ cm^{-2}: B, C; or 100 mJ cm^{-2}: D, E). 3-AT was present in (C) and (E). Similar results were obtained in a second independent experiment. [Adapted from Photochem. Photobiol. 85, 1491-6, 2009]

Table 4.2 ImageJ analysis of procaspase-3 conversion to caspases-3

	control	60 mJ cm^{-2}		100 mJ cm^{-2}	
		+ 3-AT		+ 3-AT	
	A	B	C	D	E
Procasp-3	0.647	0.836	0.667	0.815	0.321
Caspase-3	0.006	0.168	0.377	0.261	0.618

Values are expressed as ratio of procaspase-3 and caspase-3 signals to actin signal.

4.3.6 Intracellular catalase activity enhanced by CAT_{SKL}

A western blot analysis was used to confirm that treatment of P388 cells with 1000 U of CAT_{SKL} led to an increased intracellular level of catalase (Figure 4.5). ImageJ analysis confirms that there was substantial increase in intracellular catalase protein after 30 min, and only a slight additional increase when the incubation time was prolonged to 60 min (Table 4.3).

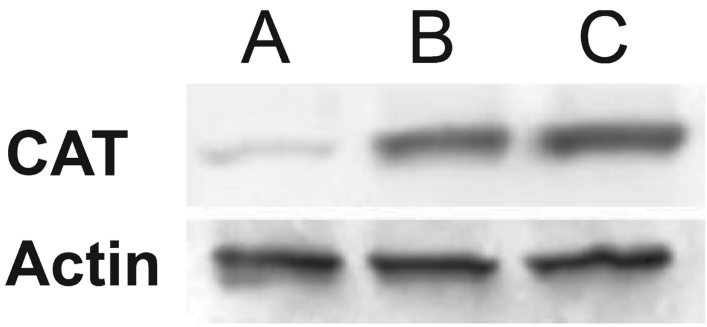

Figure 4.5 Western blots for catalase showing control levels (A) and enhanced intracellular levels of the protein after treatment of P388 cells with CAT_{SKL} (1000 U/ 5 mg of cells) for 30 min (B) or 60 min (C) at 37°C. Similar results were obtained in a second independent experiment. [Adapted from Photochem. Photobiol. 85, 1491-6, 2009]

Table 4.3 ImageJ analysis of CAT_{SKL} levels in P388 western blot

	Control	30 min	60 min
CAT_{SKL}	0.13	1.02	1.17

Values are expressed as the ratio of catalase / actin.

4.3.7 Detection of hydrogen peroxide in cell cultures

Exposure of DHR to H_2O_2 results in it's conversion to a fluorescent product, a reaction that is greatly enhanced in the presence of peroxidases (Henderson and

Chappell 1993). The system used was not sufficiently sensitive to detect H_2O_2 in control P388 cells, but could readily detect fluorescence produced directly after irradiation (Table 4.1). This fluorescence was significantly enhanced by the presence of 3-AT and decreased when CAT_{SKL} was used to enhance the catalase concentration. Iron chelation and the resulting blockage of •OH formation by BIP did not have a statistically significant effect on DHR fluorescence. These data were obtained using a multichannel analyzer and CCD device, permitting acquisition of fluorescence emission spectra averaged over 2 s. Fluorescence at the emission maximum (525 nm) was recorded. A different detection system was used to monitor the fluorogenic effect of PDT on DHR oxidation. Data shown in Figure 4.6 were obtained during the irradiation of photosensitized cell cultures and show effects of prior treatment with 3-AT or CAT_{SKL}. The fluorogenic reaction was enhanced by treatment with 3-AT and impaired after exposure of cells to CAT_{SKL}. Data were acquired as a function of time, using a photomultiplier detector in the single-photon mode. Excitation = 490 nm; emission was monitored at 525 nm every 4 s using 0.3 s time interval for each data point.

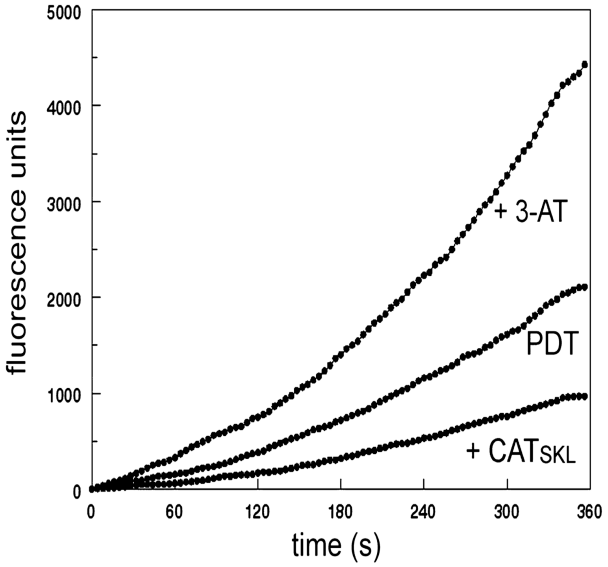

Figure 4.6 Fluorogenic effect of PDT on DHR oxidation. Fluorescence of P388 cells loaded with 1 μM DHR + 2 μM BPD (with 30 mM 3-AT or 1000 U of CAT_{SKL} present where specified) and irradiated at 690 nm for 360 s. During this time, the fluorescence signal from oxidized DHR at 525 nm was acquired using 490 nm excitation. These curves represent data for a typical experiment. Essentially the same patterns were obtained during two repetitions of this study. [Adapted from Photochem. Photobiol. 85, 1491-6, 2009]

4.3.8 Statistical treatment

Using paired one-tailed t-tests (with a sample population of 3 for all calculations) indicates that (1) in controls, treatment with either with 3-AT or CAT_{SKL} significantly altered catalase activity from the control levels ($p < 0.05$), and (2) incubation with 3-AT and CAT_{SKL} significantly altered DEVDase activity, catalase activity, DHR fluorescence and the LD_{50} dose from the values obtained with PDT alone ($p < 0.05$). Moreover, the addition of BIP had no significant effect on any PDT-induced parameter. Chelation of ferrous ion appears to offer some protection from phototoxicity and decrease in DEVDase activity, but these effects did not reach the 95% confidence level.

4.4 CONCLUSIONS

The dose–response curve for BPD-PDT (Figure 4.1) demonstrated that even a small increase in light dose can cause a substantial increase in phototoxicity. Causing such an increase by manipulating H_2O_2 formation is therefore a possibility to be considered.

Apoptosis is an irreversible process leading to cell death, and has been shown to be a predominant form of direct cell kill after PDT (Oleinick, Morris et al. 2002). Singlet oxygen is widely assumed to be the initial toxic ROS produced during PDT with most of the current photosensitizing agents in clinical use. A recent report (Kim, Rodriguez et al. 2008), using only a photosensitizer + cytochrome *c*, indicated that there were oxidation products that could not be explained by the action of $^1O_2$ alone. While a solution containing a photosensitizer and a protein may not accurately mimic the conditions that occur in cells or tissues, results reported in this study indicate that even in a simple system, multiple ROS can be detected. Kochevar et al. (2000), using HL-60 cells, found that altering irradiation conditions such that rose bengal produced either $^1O_2$

or radical species, resulted in apoptosis only under the former conditions. Assuming that this effect may also be pertinent to the cell line and photosensitizing agent used here, radical-initiated photodamage may be an inefficient method for inducing apoptosis, but might amplify the phototoxic effect(s) of $^1O_2$. [note: that later studies showing WST11 to be less efficient than NPe6 is consistent with this supposition].

Figure 4.3 demonstrates that the apoptotic response to PDT is enhanced by 3-AT and decreased when the intracellular concentration of catalase is enhanced. Changes in the apoptotic response were reflected in the conversion of procaspase-3 to the active form (Figure 4.4). Additional studies were carried out with BIP, a reagent that chelates Fe^{+2} and is therefore expected to antagonize formation of •OH *via* the Fenton reaction. These data are summarized in Table 4.1.

The ability of the CAT_{SKL} preparation to augment the cellular level of catalase was demonstrated by studies involving Western blot analysis. In the context of these studies, it is important to consider that CAT_{SKL} was specifically designed as an exogenous source of catalase activity that would migrate to the peroxisome where this enzyme is normally found (Terlecky, Koepke et al. 2006; Koepke, Nakrieko et al. 2007; Terlecky and Koepke 2007). Use of unmodified catalase will result in the appearance of enzyme activity in the cytosol where it is normally *not* found, with possible effects on signalling pathways or other anomalous changes in cell biology.

Using the fluorescent probe DHR, an estimation of H_2O_2 formation was obtained during irradiation of photosensitized P388 cells (Figure 4.5). The increase in fluorescence intensity was impaired by the presence of CAT_{SKL} and enhanced in cells previously treated with 3-AT. Fluorescence values shown in Figure 4.5 were measured with a photomultiplier-based fluorometer that permits data accrual at a single

wavelength, while results shown in Table 4.1 were obtained with a multichannel analyzer and a CCD camera. The numerical values are therefore different but the overall trends are consistent with interpretations.

In these studies, there was no significant alteration in the level of catalase activity when photosensitized cells were irradiated. This differs from results reported by (Luo, Li et al. 2006) who observed a significant decrease when keratinocytes were treated with Photofrin and then irradiated. This result could be attributed to the fact that Photofrin is a complex mixture of porphyrin monomers, dimers and higher oligomers that may localize quite differently than BPD.

Hydrogen peroxide can promote autophagy (Scherz-Shouval, Shvets et al. 2007) *via* oxidation of an amino acid on one of the proteins involved in the autophagic process. Since autophagy is expected to protect cells from low-dose PDT (Kessel and Arroyo 2007), enhanced autophagy resulting from H_2O_2 formation might be expected to decrease overall PDT efficacy, although results shown in Table 4.1 indicate otherwise. Further studies using cell lines lacking the capacity for autophagy might provide further information on the potential role of H_2O_2-induced autophagy in the overall phototoxic effect.

What conclusions can be drawn from these studies? Verma, Watt et al. (2007) proposed new strategies for promotion of PDT efficacy. One involves combination therapy with a view toward increasing susceptibility of cells to PDT. It had previously been shown that concurrent treatment with PDT + Bcl-2 antagonists resulted in enhanced photokilling (Kessel 2008). The present study suggests that, in addition to the effects of $^1O_2$ on such critical targets as anti-apoptotic Bcl-2 family proteins (Kim, Luo et al. 1999; Xue, Chiu et al. 2001) and on lysosomes (Reiners, Caruso et al. 2002),

H_2O_2 formed during PDT may also play a role in photokilling. As indicated by Figure 4.1, any phenomenon that produces even a minor promotion in PDT efficacy can have a marked effect on tumor eradication.

CHAPTER 5

EVALUATION OF DIETHYL-3-3'-(9,10-ANTHRACENEDIYL)*BIS* ACRYLATE AS A PROBE FOR SINGLET OXYGEN FORMATION DURING PHOTODYNAMIC THERAPY

5.1 INTRODUCTION

Singlet oxygen has been considered the predominant cytotoxic product formed during PDT (Weishaupt, Gomer et al. 1976; Thomas, Hall et al. 1987; Niziolek-Kierecka, Pilat et al. 2010). The 'classic' method for monitoring $^1O_2$ formation involves the detection of 1270 nm phosphorescence using a detector cooled to 77 K. This requires equipment not routinely available in many laboratories. Electron spin resonance (ESR) can also be used in conjunction with appropriate spin traps, but this can be unwieldy for studies involving cell culture. A variety of fluorescent probes have been identified that can detect different ROS, but the specificity is often less than is advertised (Bartosz 2006; Price and Kessel 2010; Zielonka and Kalyanaraman 2010). The fluorescent probe APF, initially designed to detect •OH (Setsukinai, Urano et al. 2003), can also detect the high concentrations of $^1O_2$ produced during PDT (Price, Reiners et al. 2009). But APF is also highly-sensitive to •OH, so it does not represent an ideal singlet oxygen probe.

A more selective probe for $^1O_2$ detection is SOSG, but this agent is unable to penetrate cell membranes (Flors, Fryer et al. 2006). Ogilby's group reported a procedure for promoting cellular uptake of SOSG, but reported that the ability of the probe to detect $^1O_2$ formation during PDT was unreliable (Gollmer, Arnbjerg et al. 2011). It is possible that this problem arose from their choice of the photosensitizing agent, the tetra cationic porphyrin TMPyP. This agent was reported to concentrate in nuclei

(Tada-Oikawa, Oikawa et al. 2009) and the extent of penetration of SOSG into nuclei is unknown.

A recent report has indicated the synthesis of a cell-permeable probe for $^1O_2$ (Oliveira, Severino et al. 2011). This anthracene derivative, termed diethyl-3-3'-(9,10-anthracenediyl)bis acrylate (DADB), was both highly selective for $^1O_2$ and able to cross the plasma membrane. Unlike many other ROS probes, the fluorescence of DADB is reduced by the formation of an endoperoxide when exposed to $^1O_2$.

Experiments were designed to examine the ability of DADB to detect ROS formed by a group of photosensitizing agents with different sites of sub-cellular localization. Effects of two lysosomal photosensitizers with differing patterns of ROS formation were compared: the chlorin NPe6 and the palladium bacteriopheophorbide WST11 (Mazor, Brandis et al. 2005). NPe6 is known to have a high $^1O_2$ yield upon irradiation (Spikes and Bommer 1993; Spikes and Bommer 1993), whereas WST11 produces mainly oxygen radicals upon irradiation in a relatively aqueous environment (Ashur, Goldschmidt et al. 2009).

5.2 MATERIALS AND METHODS

5.2.1 Chemicals and Reagents

NPe6 was provided by Prof Kevin M. Smith, Louisiana State University. BPD was purchased from VWR, mTHPC was obtained from Frontier Scientific and WST11 was prepared as described in (Brandis, Mazor et al. 2005). Refer to section 2.2.1 for other photosensitizers used. The synthesis of DADB was carried out as indicated in (Oliveira, Severino et al. 2011) with a minor alteration: the reaction mixture (dibromoanthracene + ethylacrylate) was maintained at 110°C for only 8 h without affecting the yield of product.

5.2.2 Cell culture

Murine hepatoma Hepa 1c1c7 cells were initially obtained from Dr. JP Whitlock Jr, Stanford University and provided by Dr. J. Reiners, Jr. These cells were maintained in αMEM (Sigma–Aldrich, St. Louis, MO) supplemented with 5% fetal bovine serum and antibiotics in a 5% CO_2 atmosphere, at 37°C.

5.2.3 Photodynamic studies in cell culture

1c1c7 cells were cultured on 22 mm glass cover slips in 5% CO_2. PDT studies were carried out after incubation with 1 μM WST11 for 16 h, 0.5 μM BPD for 1 h, 20 μM NPe6 for 1 h or 0.5 μM mTHPC for 16 h, all at 37°C. The medium was then replaced and the cells irradiated. The light source was a 600 W quartz-halogen lamp with IR radiation attenuated by a 10 cm layer of water and further limited by interference filters (±10 nm). Irradiation took place at a temperature of 15°C to inhibit initiation of apoptosis. Concentrations of the photosensitizers were adjusted so as to produce a 90% photokilling by a 270 mJ cm^{-2} light dose. The wavelengths of irradiation were 750 nm (WST11), 690 nm (BPD) and 660 nm (mTHPC and NPe6). During the final hour of the photosensitizer loading incubation, DADB was added (10 μM). LD_{90} doses for the photosensitizers employed in this study were established by clonogenic studies. Fluorescence images were acquired directly after irradiation.

5.2.4 Phase-contrast and fluorescence microscopy.

Images were acquired with a Nikon E-600 microscope using a Rolera EMCCD camera (QImaging, Surrey, BC, Canada). DADB fluorescence centered at 525 nm was determined using 360–400 nm excitation. A 600 nm low-pass filter was inserted into the emission path to eliminate fluorescence emission from the photosensitizing agents. The acquisition time for each fluorescence image was 100 ms. The resulting images were

acquired and analyzed using the 'region statistics' program (MetaMorph, see section 3.2.9). Data are reported in terms of average pixel density ± SD for images involving at least 30 cells. Additional studies were carried out to assess the variation of this value in replicate images.

5.2.5 Oxidation of DADB.

To assess the stability of DADB to irradiation during fluorescence microscopy, stability of this agent to the light used in image acquisition was first assessed. Two successive 100 ms exposures were used to determine whether there was a loss of fluorescence after a 100 ms exposure to exciting light on the stage. As an additional stability test, cells loaded with DADB were exposed to exciting light for 15 s, and an image acquired. This is far longer than the 100 ms exposure time, and provided an estimate of probe stability to the UV excitation beam. The next experiment involved the determination of the ability of photosensitizers to alter DADB fluorescence. This was carried out by measuring the change in pixel brightness as a result of irradiation of photosensitized cells containing DADB.

5.2.6 Statistical analyses

To determine any significance of the effects of PDT on DADB fluorescence, unpaired one-tailed t-tests were run using the mean ± SD of the pixel intensity and the number of cells in the field as the sample size, n, for standardization.

5.3 RESULTS AND DISCUSSION

5.3.1 DADB: labelling pattern

Incubation of 1c1c7 cells with 10 μM DADB for 60 min led to a labelling pattern that appears to involve intracellular membranes (Figure 5.1). The fluorescence labelling pattern did not appear to involve any specific organelle population, although nuclear

labelling was negligible.

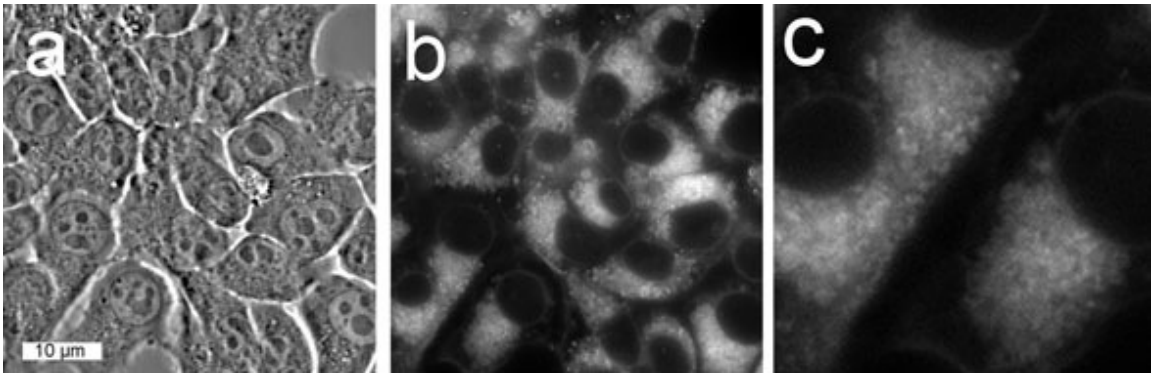

Figure 5.1 Phase-contrast (a) and fluorescence images (b and c) showing the localization of DADB in 1c1c7 cells following a 1 h incubation with a 10 µM DADB concentration. Panel (c) is an enlargement of the lower left portion of panel (b). Photographs are representative of observations for three independent experiments. [Adapted from Photochem. Photobiol. 88, 717-20, 2012]

5.3.2 Intrinsic DADB oxidation

Mammalian cells are known to form ROS, including $^1O_2$, during UV irradiation (Tyrrell and Pidoux 1989). To examine the effect of image acquisition on DADB, cells were used that had been incubated with the probe alone. No significant decrease in the fluorescence signal was observed after a 100 ms exposure interval (c.f. Figure 5.2 a, b; Figure 5.4). A decrease in fluorescence was, however, detected when cells loaded with

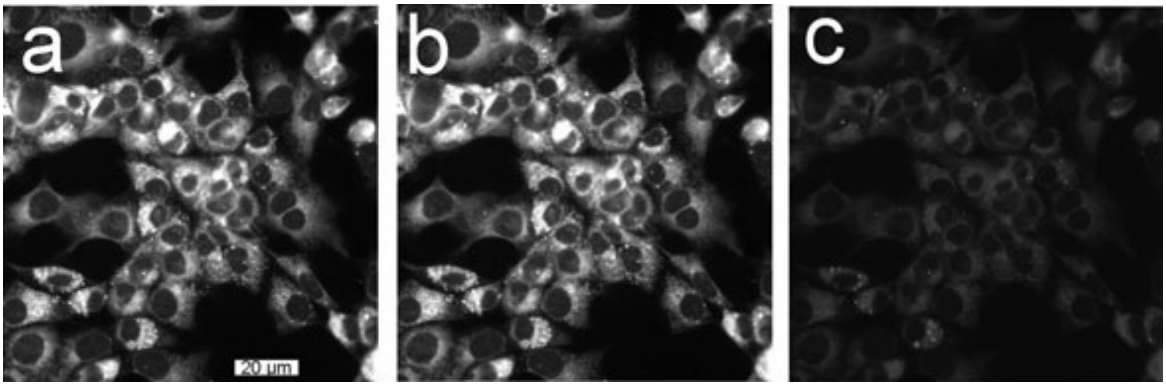

Figure 5.2 Fluorescence intensity of intracellular DADB as a function of the time of exposure of cells to illumination on the microscope stage (380– 400 nm). Panels (a and b) represent two sequential exposures of 100 ms each, to test for photobleaching during image acquisition. Panel (c) showed the image captured by a 100 ms exposure after 15 s of irradiation on the microscope stage. Photographs are representative of observations for three independent experiments. [Adapted from Photochem. Photobiol. 88, 717-20, 2012]

DADB cells were exposed to UV light from the excitation source on the microscope stage for 15 s before image acquisition (Figure 5.2 c; Figure 5.4).

5.3.3 Effects of varying the ROS on DADB fluorescence

Both NPe6 and WST11 localize in lysosomes, but produce different ROS upon irradiation (Kessel and Price 2012). An LD_{90} PDT dose led to a barely detectable effect on DADB fluorescence when WST11 was employed (Figure 5.3, C). In contrast, a significant loss of DADB fluorescence was observed with NPe6 (Figure 5.3, D), an agent known to produce a substantial $^1O_2$ yield upon irradiation (Spikes and Bommer 1993). A 'region statistics' analysis (see section 3.2.9) of pixel brightness in these images showed values of 22.7 ± 2.3 (background), 85.6 ± 4.8 (DADB control) 85 ± 4.7 (PDT using WST11) and 55 ± 2.4 (NPe6). Both of the latter images were acquired using LD_{90} PDT doses. These data indicated that NPe6, but not WST11, was associated with the decreased DADB fluorescence derived from singlet oxygen formation. A more

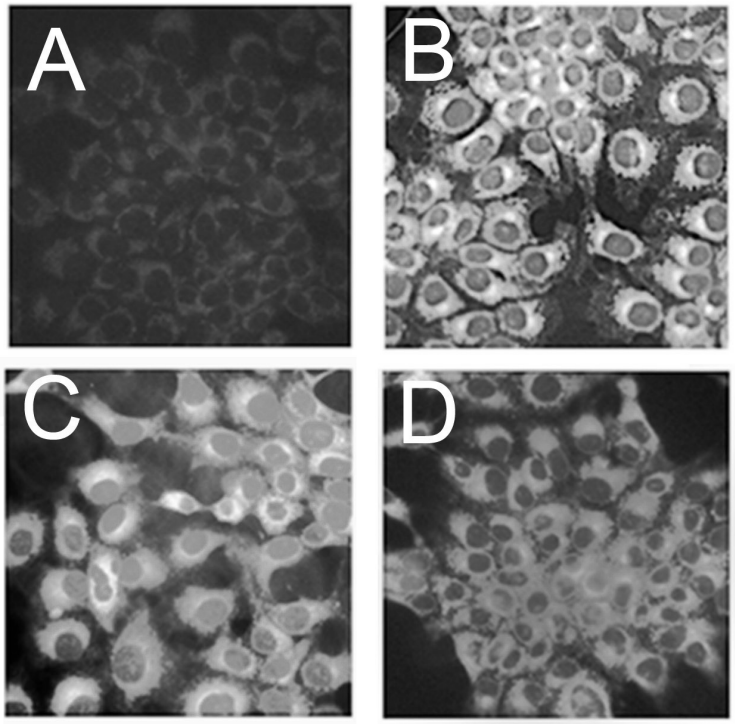

Figure 5.3 Effect of ROS formation on DADB fluorescence: (A) background fluorescence of cells; (B) control DADB fluorescence; (C) DADB fluorescence following an LD_{90} PDT dose using WST11; (D) a similar study with NPe6. Photographs are representative of observations for three independent experiments.

detailed analysis involving other photosensitizing agents and multiple trials was then carried out.

5.3.4 Loss of DADB fluorescence after PDT using different photosensitizing agents

Photodynamic therapy under LD_{90} conditions with two other photosensitizing agents also led to a loss of DADB fluorescence (Figure 5.4). For this study, mTHPC, a photosensitizer targets ER and golgi (Marchal, Francois et al. 2007) and BPD, an agent that targets mitochondria (Peng, Chang et al. 2005), were utilized. Results obtained with WST11 and NPe6 are also shown in this figure. The data shown represent the result of 'region statistics' analysis of single images, followed by an analysis of images from three replicate studies where only the mean pixel brightness value ± SD was determined.

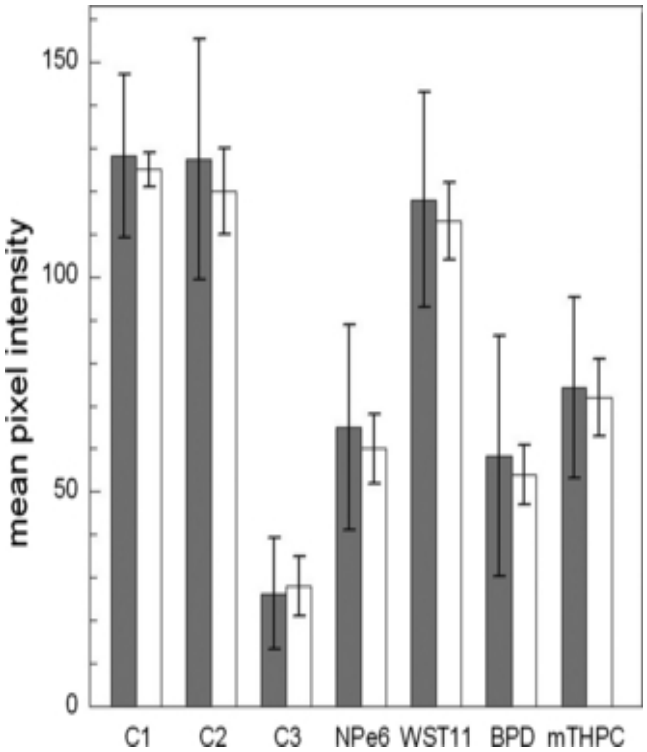

Figure 5.4 DADB oxidation by singlet oxygen as indicated by pixel brightness. All acquisitions involved a 100 ms exposure interval. Gray bars: mean pixel intensity of DADB in a typical experiment involving 50 ± 5 control cells or cells after PDT. C1, C2 = two sequential images of the same field to test for loss of fluorescence during acquisition; C3 = an image acquired after a 15 s exposure of cells to the excitation beam on the microscope stage; NPe6, WST11, BPD, mTHPC = images of cells after LD_{90} PDT doses with specified photosensitizers. Open bars represent the mean ± SD for three separate experiments where only the mean pixel intensity of the images was evaluated with the SD derived from these values. [Adapted from Photochem. Photobiol. 88, 717-20, 2012]

5.3.5 Statistical considerations

The grey error bars shown in Figure 5.4 represent the variation in pixel intensity in the cytoplasmic region of cells in the microscope field, not the variation in the mean value for pixel intensity for replicate determinations. The extent of the error bars indicate that there are subcellular regions with differing pixel brightness in all the images. This variation can readily be observed in a magnified image of a portion of Figure 5.1b, shown in panel c. This variation is typical but does not appear to detract from the utility of this probe. When the mean pixel density was measured in triplicate samples, the average value of pixel intensity showed a much smaller SD (open bars shown in Figure 5.4) than the analysis of a single image.

5.4 CONCLUSIONS

DADB can monitor the formation of $^1O_2$ by several photosensitizing agents regardless of their site of initial subcellular localization. A high degree of specificity of DADB for singlet oxygen detection was indicated in Oliveira, Severino et al. (2011), as was the ability of this agent to penetrate cell membranes. The loss of DADB fluorescence during PDT in a cell-free system established the ability of this agent to interact with $^1O_2$, but did not provide an estimate of sensitivity in the context of PDT. Using BPD, mTHPC or NPe6, a similar loss of DADB fluorescence was observed at equitoxic PDT doses (Figure 5.4). Qualitative comparisons are readily feasible, e.g., demonstrating that an LD_{90} PDT dose with the lysosomal targeting photosensitizer NPe6 produces substantially more $^1O_2$ than did a comparable PDT dose with WST11. The latter also targets lysosomes (Kessel, Price et al. 2012), but produces mainly oxygen radicals (Ashur, Goldschmidt et al. 2009). Other procedures for $^1O_2$ detection are available, e.g., measuring the 1270 nm $^1O_2$ signal (Baker and Kanofsky 1991).

Geiger, Korytowski et al. (1997) has described a chromatographic procedure that measures the conversion of cholesterol to a product that is uniquely formed by the action of $^1O_2$. The development of a cell-permeable fluorescent probe, if adequately sensitive, would place $^1O_2$ measurements within the reach of laboratories with conventional fluorescence microscopy facilities. Quantitative aspects of the analysis depend on how well $^1O_2$ generated at different subcellular loci can interact with DADB and how well DADB can compete with biological substrates for oxidation. There was a broad spectrum of pixel intensities within a single field. The standard deviation value was as large as 30% of the mean in untreated cells and cells that had been photosensitized and irradiated (Figure 5.4). Areas selected for the thresholding program showed a considerable variation in pixel intensity, but the mean pixel intensity measurement of several images appears to provide a reproducible indication of the level of probe oxidation. An alternative approach is discussed in Oliveira, Severino et al. (2011): GC／MS analysis could provide an indication of DADB oxidation free from errors implicit in the thresholding process. These data indicate that DADB can successfully be used as a fluorescence probe for singlet oxygen formation in live cells. Although excitation in the UV can also elicit a loss of DADB fluorescence even in the absence of a photosensitizing agent, the exposure times were sufficiently small so that this problem was avoided.

CHAPTER 6

WST11 AND NPe6: EFFECTS OF OXYGENATION LEVELS ON PHOTOSENSITIZING EFFICACY

6.1 INTRODUCTION

Clinical evidence suggests tumor hypoxia can lead to resistance to both radio- and chemotherapy (Moulder and Rockwell 1987; Teicher 1994; Castano, Demidova et al. 2005; Moeller, Richardson et al. 2007). This had led researchers to find procedures to improve tumor oxygenation. The presence of dissolved oxygen in the target tissue is one of the primary components for treatment with PDT. Studies have been conducted since the mid-1980s on the requirement for oxygen in the photokilling of cells. Moan's group showed that with HPD-sensitized NHIK 3025 cells, photosensitivity was reduced by 50% of its maximal effectiveness when cells were incubated and irradiated in 1% oxygen (Moan and Sommer 1985). Henderson showed similar results with Photofrin II and RIF cells using 1% O_2 (Henderson and Fingar 1987). Both articles noted that the treatment of tumors with anoxic regions still showed high cure rates (or favourable treatment outcomes) and concluded that the tumor cell inactivation in these regions must be the result of a mechanism(s) other than direct PDT cytotoxicity. While shutdown of tumor vasculature is commonly seen with the use of several photosensitizers and is believed to play a role in the overall tumor destruction (McMahon, Wieman et al. 1994; Fingar 1996; Fingar, Kik et al. 1999), tumor cell kill in regions of hypoxia was attributed to an unknown secondary method (Henderson and Fingar 1987; Fingar, Wieman et al. 1992).

Once it was shown that NPe6 and WST11 both localized in lysosomes but produced different ROS upon irradiation, a series of experiments was designed to

determine whether formation of singlet oxygen vs. oxygen radical species were equally sensitive to hypoxia.

6.2 MATERIALS AND METHODS

6.2.1 Chemicals and Reagents

Refer to sections 2.2.1 and 5.2.1 for probes and photosensitizers used in these experiments. Nitrogen and nitrogen-oxygen mixtures were provided by Praxair.

6.2.2 Cell culture

See section 5.2.2 for details on the maintenance of the murine 1c1c7 cell line.

6.2.3 Clonogenic assays

A suspension of 1c1c7 cells was diluted so as to contain approximately 100 cells per 1ml of media. Aliquots of 3 ml were then added to 60 mm^2 tissue culture dishes. One group of dishes was then incubated at 37º C in a 5% CO_2 incubator for 24 h while a second set was similarly incubated at 37ºC in a sealed BioSpherix incubator equilibrated with 5% CO_2, 1% oxygen. HIF1-α upregulation was verified by western blot to check for hypoxic status.

6.2.4 Photosensitization and analysis of colony formation

Dishes from the normoxic and hypoxic incubators were then incubated with WST11 (2 μM, 16 hr) or NPe6 (20 μM, 1 hr), the media replaced with fresh media that had been equilibrated in an atmosphere of 20% or 1% oxygen, and finally irradiated for graded intervals (section 2.2.4). After irradiation, all dishes were returned to the 5% CO_2 incubator for 7–9 days.

Numbers of colonies were then determined using an Oxford Optronix GelCount™ electronic colony counting system. Data reported represent results obtained with triplicate samples and are shown as % of surviving colonies using the untreated controls

as 100%.

6.2.5 Photobleaching studies

These studies were carried out in 3 ml volumes of 10 mM phosphate buffer pH 7. An atmosphere of 1% oxygen was obtained by equilibrating autoclaved buffer with 99% nitrogen:1% oxygen for 30 min. To achieve a minimal level of oxygen, a gas composed of 99.99% nitrogen was passed through a high capacity oxygen trap (RESTEK, Bellfonte, PA) with PVC plastic tubing used for connections to further reduce contamination by atmospheric oxygen. Initial optical densities at 654 nm (NPe6) or 748 nm (WST11) were 0.100 ± 0.005. Either of two fluorescent probes, APF or SOSG, was present at 2 μM concentrations, where specified.

Glass cuvettes with polished, transparent bottoms were irradiated from below using laser diodes (662 nm for NPe6; 750 nm for WST11) at a power of 100 mW. Under these conditions, a 10 second irradiation corresponds to 1 joule. During the irradiation process, gas mixtures or air were constantly bubbled into the cuvette. Photosensitizer spectra were obtained using a Shimadzu Biospec-1601 spectrophotometer and log of optimal emission was potted against time of irradiation. The spectrum of the probe fluorescence was obtained using an Instaspec X CCD (Oriel/Newport) detector, with optimal fluorescence plotted against time of irradiation. The optical density of the photosensitizer and the fluorescence of the probe were determined after irradiations for 15 or 30 seconds.

6.2.6 Measurement of oxygenation levels.

Phosphate buffers equilibrated with different levels of oxygen were tested for levels of dissolved oxygen using the Winkler procedure (Helm, Jalukse et al. 2009). Triplicate assays were carried out using reagent solutions that had been equilibrated

with the specified oxygen mixtures.

6.2.7 Statistical analyses and implications

An unpaired two-tailed t-test was performed on the clonogenic data to determine whether the oxygenation level had a significant effect on phototoxicity. A simple linear regression analysis was also performed to determine whether the different oxygenation conditions resulted in data that could be fitted to two regression lines or to a single line. The probability that the linear regression lines represented two different sets of data or could be derived from a single set was then calculated.

6.3 RESULTS AND DISCUSSION

6.3.1 Clonogenic data

The clonogenic results obtained showed different sensitivity to the oxygenation level; photosensitization with WST11 showed a diminished rate of photokilling when the percentage of oxygen in the system was lowered from 20% to 1% (Figure 6.1, Panel A). The light dose required for a 50% loss of viability changed from 180 to 360 mJ cm^{-2}.

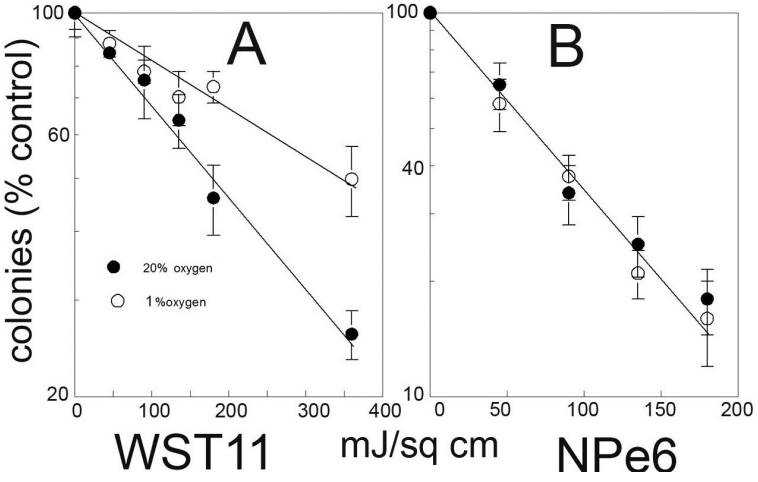

Figure 6.1 Clonogenic analysis of murine 1c1c7 photosensitized with WST11 (A) and NPe6 (B). Cells were incubated and irradiated in 20% (closed circles) or 1% (open circles) oxygen. Error bars represent SD for 3 determinations. Similar results were observed in a second independent experiment.

The regression values (r^2) were 0.94 (20 % oxygen) and 0.93 (1% oxygen). Of the values in the chart, only those for 180 and 360 mJ cm^{-2} were significantly different (p < 0.05) for the two oxygenation levels. In contrast, with NPe6, there was no difference in

the degree of photokilling in 1% vs. 20% oxygen (Figure 6.1, Panel B). Since PDT is carried out with a view toward maximum tumor eradication, we considered the effects at the higher light doses to be more pertinent indexes, or indicators of the effect of the oxygenation level on efficacy. Data obtained with WST11 at 1% vs. 20% oxygenation was found to represent two separate regression lines at a 95% confidence level.

6.3.2 Dissolved oxygen levels

An analysis using the Winkler procedure indicated that buffer prepared under atmospheric oxygen contained 8.9 ± 0.3 mg/l of dissolved oxygen (280 μM). Buffer equilibrated with 1% oxygen showed a level of 0.46 ± 0.02 mg/l of oxygen (14.5 μM). The analysis of buffer degassed with 99.99% nitrogen indicated an oxygenation level of 0.005 ± 0.001 mg/l (160 nM).

6.3.3 Photobleaching and ROS production

Photobleaching of photosensitizing agents provides information on levels of ROS produced during irradiation that results in alterations in UV/VIS spectra. Fluorescent probes were also used to compare rates of formation of $^1O_2$ and •OH. These studies were carried out in cell-free systems so as to provide information on photochemical processes that could be correlated with clonogenic photokilling data.

The choice of fluorescent probe was dictated by prior experience with individual products. DHR is responsive to a variety of ROS, but was found be unstable to light of almost any wavelength if the intensity was sufficiently high (as would occur during photobleaching studies). A similar phenomenon has been observed with reduced DCF (Afzal, Matsugo et al. 2003). SOSG and APF were unaffected by light intensities used in these studies.

Photobleaching and photoproduct formation were assessed by

spectrophotometric studies (Figure 6.2). At the low concentration of the photosensitizers used here (optical density = 0.1), photoproducts were formed, as indicated by progressive changes in the absorbance spectra, even in 0.01% oxygen.

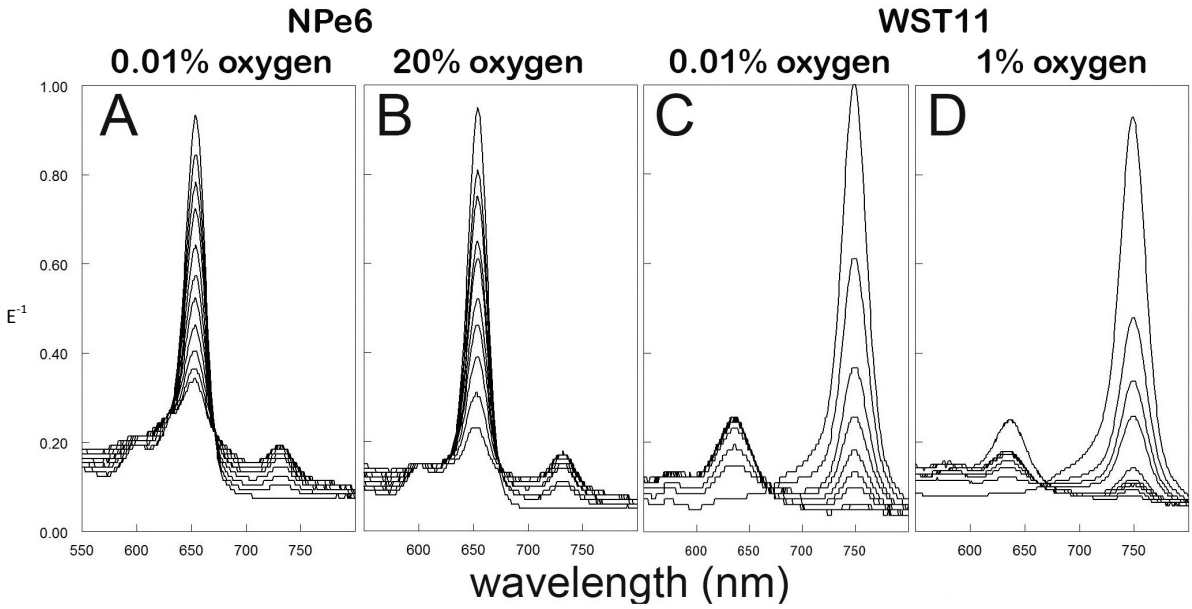

Figure 6.2 Photobleaching analysis of NPe6 in (A) and (B) and WST11 in (C) and (D) after irradiation in buffers equilibrated with 0.01% (A, C) or 20% (B, D) oxygen. Initial absorbance peaks for NPe6 at 650 nm and WST11 at 750 nm both decrease during the subsequent irradiation periods. Similar results were observed in three independent experiments.

Rates of photobleaching were assessed to provide a kinetic study (Figure 6.3). Panel A shows that photobleaching of NPe6 was initially linear regardless of the level of oxygenation (20%, 1%, 0.01%). At the higher light doses, the fall-off in photobleaching can be attributed to depletion of oxygen in the system. SOSG fluorescence formation under all three conditions showed a similar pattern; the initial rate was essentially identical regardless of the oxygenation level. These results suggest that the excited state of NPe6 is very successful at scavenging even very low levels of dissolved oxygen to form $^1O_2$. In contrast, Figure 6.3(B) shows that this is not true when APF fluorescence was used to provide an index of •OH formation. It appears that NPe6

does produce •OH, but that the rate of production is affected by the oxygen concentration in the system. APF can also detect $^1O_2$ (Price, Reiners et al. 2009), but in view of the very high yield of $^1O_2$ from NPe6 (Spikes and Bommer 1993), together with the 200-fold greater sensitivity of APF to •OH than to $^1O_2$ (Setsukinai, Urano et al. 2003), it appears that APF and SOSG can be used to distinguish between these species. It is also noteworthy that patterns of responsiveness to the oxygenation level for these two probes were substantially different with NPe6: the fluorogenic interaction with APF was much more dependent on the level of oxygenation than the interaction with SOSG.

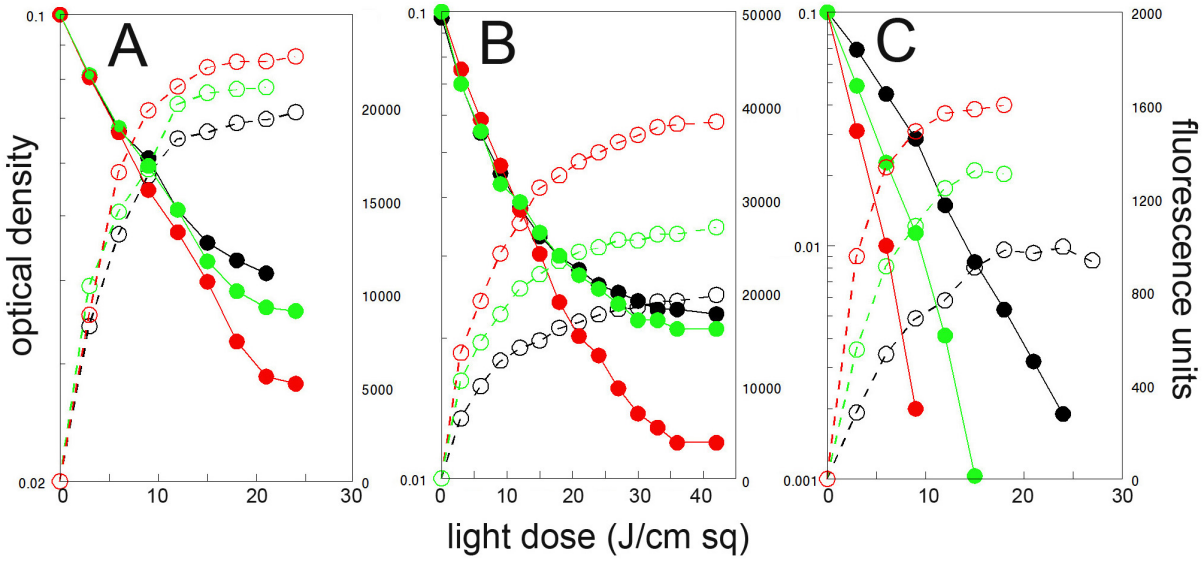

Figure 6.3 Photobleaching and fluorogenic probe analysis. A, NPe6, SOSG; B, NPe6, APF; C, WST11, APF. Closed circles represent photobleaching as determined by measuring optical density at 655 nm (NPe6) or 750 nm (WST11) as irradiation proceeded. Open circles show the fluorogenic effect of irradiation. Red = 20% oxygen; Green = 1% oxygen; Black = 0.01% oxygen. Similar results were observed in three independent experiments.

WST11 proved to be more sensitive to photobleaching than NPe6 (Figure 6.3 C). In 20% O_2, WST11 was photobleached rapidly, but even the initial rate diminished when the oxygenation level was decreased. The appearance of APF fluorescence also

diminished in an oxygen level-dependent manner, as was observed with NPe6. Photobleaching of WST11 was also observed in the deoxygenated buffer and continued even after APF fluorescence was no longer increasing. This result suggests that WST11 photobleaching independent of •OH formation can occur. Since WST11 does not form singlet oxygen upon irradiation in an aqueous environment (Ashur, Goldschmidt et al. 2009), irradiation did not yield a fluorogenic interaction with SOSG (not shown).

6.4 CONCLUSIONS

Data shown in Figurer 6.3 indicate that the rate of photochemical reactions leading to the formation of •OH is more dependent on the level of oxygenation than are reactions that result in formation of $^1O_2$. The greater efficacy of NPe6 under hypoxic conditions is therefore associated with a minimal effect of hypoxia on singlet oxygen formation, and a corresponding minimal effect on photobleaching. Formation of •OH by NPe6 was more sensitive to the level of oxygenation, but this species appears to play a minor role in photobleaching processes, and in photokilling.

In contrast, the greater sensitivity of photokilling by WST11 to hypoxia was associated with a corresponding decrease in •OH formation under hypoxic conditions. This might be considered as a potential drawback to the use of WST11 in the clinic, but the current clinical protocols involve irradiation only when WST11 is still in the circulation. Under such conditions, hypoxia is unlikely to be a factor. In these protocols, WST11 PDT leads only to vascular shutdown since an insufficient time is allowed for this agent to penetrate into tissues.

The statistical treatment of data shown in Figure 6.1 indicated that the WST photokilling data could be represented by two different regression lines, at the 95%

confidence level. In all studies involving cells, oxygen, light and clonogenic efficiency, there will always be intrinsic and extrinsic errors. In order to refine the system and examine effects of oxygenation where the probability for error was minimal, we turned to photobleaching studies in a cell-free system. These showed that production of •OH from either photosensitizer was more dependent on the level of oxygenation than was production of $^1O_2$ from NPe6. This result provides a mechanism for interpretation of the clonogenic results.

CHAPTER 7

SUMMARY

The presence of oxygen is one of the three essential components of PDT. Photosensitizers localize at a variety of different sub-cellular loci (Kessel 2004). Gorman and Rodgers (1992) proposed that 'while photosensitizers may be restricted to cellular compartments, upon being generated the all-pervasive oxygen species have finite possibilities of contacting oxidizable targets either in the immediate area of generation or across an interface.' This is only partially accurate; singlet oxygen and •OH will react only with substrates in their immediate vicinity. Moan estimated that $^1O_2$ can diffuse at most 0.02 microns from the site of formation (Moan and Berg 1991; Moan and Peng 2003). Other species, e.g. hydrogen peroxide, will likely persist for much longer times.

The research shown here has revealed several new findings relating to the role of ROS in the direct tumor cell photokilling by PDT. Singlet oxygen was initially considered as the predominant ROS formed in photosensitized cells. There has been only limited consideration shown for the role(s) of the oxygen radicals and hydrogen peroxide in the phototoxicity of PDT. Moreover, delineation of ROS can be difficult.

The specificity of several commercially available fluorogenic ROS probes was examined with a view toward providing an accessible means for testing for formation of different in a typical laboratory setting. Procedures involving detection of 1270 nm singlet oxygen phosphorescence, or use of ESR to distinguish among ROS may be highly accurate, but these methods are not readily adapted to cell-culture studies and involve specialized (and very expensive) equipment. The fluorescent ROS probes are simpler and less expensive to use, but are often assigned by their suppliers a much

greater specificity than can be justified. A few probes were identified whose specificity in the context of PDT was suitable. The most useful were APF (•OH >> $^1O_2$) and DADB (cell-permeable and highly specific for $^1O_2$). SOSG, specific for singlet oxygen but impermeable to cells, was also useful, but only for studies in cell-free systems. Several other fluorogenic ROS probes could not delineate among different reactive species in a cell-free system, they were therefore considered to be poor candidates for detecting *specific* ROS species in cell culture.

Methods for altering the concentration of ROS formed during PDT may provide a practicable method improving the efficacy of PDT. Superoxide might be another target for manipulation in future studies (see Figure 1.1); several SOD mimics and inhibitors have been used to alter levels of this ROS in cell culture. In studies reported here, formation and destruction of hydrogen peroxide were altered with a catalase antagonist (3-AT) and an exogenous catalase source (CAT_{SKL}), respectively. Studies with these agents permitted the demonstration of a role of this species as a factor in PDT efficacy. This work indicated that formation of singlet oxygen was not the sole determinant of PDT photokilling. It is not clear whether H_2O_2 was itself the pertinent cytotoxic ROS, or whether this effect derives, at least in part, from subsequent conversion to •OH, a more reactive ROS. Future studies in this area could be directed toward identification of a safe and effective short-term catalase antagonist as a means for enhancing PDT efficacy.

Phototoxic properties of singlet oxygen vs. oxygen radicals were assessed using NPe6 and WST11. Both localize in lysosomes but produce different ROS upon irradiation. Either was effective under normoxic conditions, but NPe6 efficacy was less sensitive to hypoxia than was WST11. This was traced to a correlation between oxygen

radical formation and the level of oxygenation that applies only to WST11. These results indicate that NPe6 would be the more effective agent for direct photokilling in hypoxic loci. It must, however, be noted that WST11 protocols currently involve irradiation while the agent is in the circulation, so this difference is not likely to affect efficacy. The efficacy of sensitizers that yield only oxygen radicals upon irradiation could be of limited use for treating hypoxic tumors where direct cell kill is required. In this regard, it is interesting to note that Moan and Sommer (1985) demonstrated that hematoporphyrin and HPD lost their efficacy for photokilling when the oxygen level fell to 1%. It is therefore possible that NPe6 represents a class of photosensitizing agents that can mediate phototoxic effects even at very low oxygen levels.

Hypoxic tumors have multiple survival pathways upregulated that may promote resistance to many current therapeutic modalities (Shannon, Bouchier-Hayes et al. 2003). PDT involving 5-ethylamino-9-diethyl-aminobenzo[a]phenothiazinium chloride (EtNBS) has also been shown to be useful in the treatment of ovarian tumor nodules in vitro under extreme hypoxic conditions (Evans, Abu-Yousif et al. 2011). EtNBS therefore appears to be another representative of the class of photosensitizers that, like NPe6, may be able to create cytotoxic ROS even at low tissue levels of oxygenation.

Studies reported here suggest that screening and testing of photosentizers (both current and in development) under both normoxic and hypoxic conditions is important for drug development. In this regard, it is important to remember that normal and malignant tissues will only rarely see an oxygenation level of 20%, the condition used for many tissue-culture experiments. More pertinent results will be obtained in oxygenation levels more closely approximating what is found in vivo, e.g., 5% or less.

APPENDIX

Credit Statement

Portions of the text in Chapters 2–5 and associated figures were adapted from prior publications and were used with permission from the publishers: John Wiley & Sons (Hoboken NJ; Photochem. Photobiol.) and SPIE (Bellingham, WA, J Biomed. Opt.)

REFERENCES

1. Afzal, M., S. Matsugo, et al. (2003). "Method to overcome photoreaction, a serious drawback to the use of dichlorofluorescin in evaluation of reactive oxygen species." Biochem Biophys Res Commun 304(4): 619-624.
2. Agostinis, P., K. Berg, et al. (2011). "Photodynamic therapy of cancer: an update." CA Cancer J Clin 61(4): 250-281.
3. Allison, R. R., G. H. Downie, et al. (2004). "Photosensitizers in clinical PDT." Photodiagnosis Photodyn Ther 1(1): 27-42.
4. Andrzejak, M., M. Price, et al. (2011). "Apoptotic and autophagic responses to photodynamic therapy in 1c1c7 murine hepatoma cells." Autophagy 7(9): 979-984.
5. Ashur, I., R. Goldschmidt, et al. (2009). "Photocatalytic generation of oxygen radicals by the water-soluble bacteriochlorophyll derivative WST11, noncovalently bound to serum albumin." J Phys Chem A 113(28): 8027-8037.
6. Baker, A. and J. R. Kanofsky (1991). "Direct observation of singlet oxygen phosphorescence at 1270 nm from L1210 leukemia cells exposed to polyporphyrin and light." Arch Biochem Biophys 286(1): 70-75.
7. Bartosz, G. (2006). "Use of spectroscopic probes for detection of reactive oxygen species." Clin Chim Acta 368(1-2): 53-76.
8. Brandis, A., O. Mazor, et al. (2005). "Novel water-soluble bacteriochlorophyll derivatives for vascular-targeted photodynamic therapy: synthesis, solubility, phototoxicity and the effect of serum proteins." Photochem Photobiol 81(4): 983-993.
9. Breuer, W., S. Epsztejn, et al. (1995). "Iron acquired from transferrin by K562

cells is delivered into a cytoplasmic pool of chelatable iron(II)." J Biol Chem 270(41): 24209-24215.

10. Cai, S. X., H. Z. Zhang, et al. (2001). "Design and synthesis of rhodamine 110 derivative and caspase-3 substrate for enzyme and cell-based fluorescent assay." Bioorg Med Chem Lett 11(1): 39-42.

11. Castano, A. P., T. N. Demidova, et al. (2004). "Mechanisms in photodynamic therapy: Part one—photosensitizers, photochemistry and cellular localization." Photodiagnosis Photodyn Ther 1(4): 279-293.

12. Castano, A. P., T. N. Demidova, et al. (2005). "Mechanisms in photodynamic therapy: Part three—Photosensitizer pharmacokinetics, biodistribution, tumor localization and modes of tumor destruction." Photodiagnosis Photodyn Ther 2(2): 91-106.

13. Castano, A. P., T. N. Demidova, et al. (2005). "Mechanisms in photodynamic therapy: Part two—cellular signaling, cell metabolism and modes of cell death." Photodiagnosis Photodyn Ther 2(1): 1-23.

14. Chekulayeva, L. V., I. N. Shevchuk, et al. (2006). "Hydrogen peroxide, superoxide, and hydroxyl radicals are involved in the phototoxic action of hematoporphyrin derivative against tumor cells." J Environ Pathol Toxicol Oncol 25(1-2): 51-77.

15. Crow, J. P. (1997). "Dichlorodihydrofluorescein and dihydrorhodamine 123 are sensitive indicators of peroxynitrite in vitro: implications for intracellular measurement of reactive nitrogen and oxygen species." Nitric Oxide 1(2): 145-157.

16. Cuenca, R. E., R. R. Allison, et al. (2004). "Breast cancer with chest wall

progression: treatment with photodynamic therapy." Ann Surg Oncol 11(3): 322-327.

17. Dolmans, D. E., D. Fukumura, et al. (2003). "Photodynamic therapy for cancer." Nat Rev Cancer 3(5): 380-387.

18. Donohue, E., A. Tovey, et al. (2011). "Inhibition of autophagosome formation by the benzoporphyrin derivative verteporfin." J Biol Chem 286(9): 7290-7300.

19. Doshi, J. M., D. Tian, et al. (2007). "Ethyl-2-amino-6-bromo-4-(1-cyano-2-ethoxy-2-oxoethyl)-4H- chromene-3-carboxylate (HA 14-1), a prototype small-molecule antagonist against antiapoptotic Bcl-2 proteins, decomposes to generate reactive oxygen species that induce apoptosis." Mol Pharm 4(6): 919-928.

20. Dougherty, T. J., C. J. Gomer, et al. (1998). "Photodynamic therapy." J Natl Cancer Inst 90(12): 889-905.

21. Entman, M. L., K. Youker, et al. (1992). "Neutrophil induced oxidative injury of cardiac myocytes. A compartmented system requiring CD11b/CD18-ICAM-1 adherence." J Clin Invest 90(4): 1335-1345.

22. Evans, C. L., A. O. Abu-Yousif, et al. (2011). "Killing hypoxic cell populations in a 3D tumor model with EtNBS-PDT." PLoS One 6(8): e23434.

23. Faurschou, A. and R. Gniadecki (2008). "TNF-alpha stimulates Akt by a distinct aPKC-dependent pathway in premalignant keratinocytes." Exp Dermatol 17(12): 992-997.

24. Fenton, H. J. H. (1984). "Oxidation of tartaric acid in presence iron." J. Chem. Soc., Trans 65: 899-910.

25. Fingar, V. H. (1996). "Vascular effects of photodynamic therapy." J Clin Laser Med Surg 14(5): 323-328.

26. Fingar, V. H., P. K. Kik, et al. (1999). "Analysis of acute vascular damage after photodynamic therapy using benzoporphyrin derivative (BPD)." Br J Cancer 79(11-12): 1702-1708.

27. Fingar, V. H., T. J. Wieman, et al. (1992). "Implications of a pre-existing tumor hypoxic fraction on photodynamic therapy." J Surg Res 53(5): 524-528.

28. Flors, C., M. J. Fryer, et al. (2006). "Imaging the production of singlet oxygen in vivo using a new fluorescent sensor, Singlet Oxygen Sensor Green." J Exp Bot 57(8): 1725-1734.

29. Foote, C. S. (1991). "Definition of type I and type II photosensitized oxidation." Photochem Photobiol 54(5): 659.

30. Franco, R., M. I. Panayiotidis, et al. (2007). "Glutathione depletion is necessary for apoptosis in lymphoid cells independent of reactive oxygen species formation." J Biol Chem 282(42): 30452-30465.

31. Fujimoto, S. (1965). "Studies on estimation of catalase activity by the use of titanium sulfate." Cancer Res 25: 534-538.

32. Geiger, P. G., W. Korytowski, et al. (1997). "Lipid peroxidation in photodynamically stressed mammalian cells: use of cholesterol hydroperoxides as mechanistic reporters." Free Radic Biol Med 23(1): 57-68.

33. Girotti, A. W. (1998). "Lipid hydroperoxide generation, turnover, and effector action in biological systems." J Lipid Res 39(8): 1529-1542.

34. Gollmer, A., J. Arnbjerg, et al. (2011). "Singlet Oxygen Sensor Green(R): photochemical behavior in solution and in a mammalian cell." Photochem Photobiol 87(3): 671-679.

35. Gorman, A. A. and M. A. Rodgers (1992). "Current perspectives of singlet

oxygen detection in biological environments." J Photochem Photobiol B 14(3): 159-176.

36. Gorman, A. A. and Rogers (1989). Singlet Oxygen. Boca Raton, FL, CRC Press.

37. Gorris, H. H. and D. R. Walt (2009). "Mechanistic aspects of horseradish peroxidase elucidated through single-molecule studies." J Am Chem Soc 131(17): 6277-6282.

38. Gozuacik, D. and A. Kimchi (2007). "Autophagy and cell death." Curr Top Dev Biol 78: 217-245.

39. Granville, D. J., J. G. Levy, et al. (1997). "Photodynamic therapy induces caspase-3 activation in HL-60 cells." Cell Death Differ 4(7): 623-628.

40. Grutter, M. G. (2000). "Caspases: key players in programmed cell death." Curr Opin Struct Biol 10(6): 649-655.

41. Hamblin, M. R. and E. L. Newman (1994). "On the mechanism of the tumour-localising effect in photodynamic therapy." J Photochem Photobiol B 23(1): 3-8.

42. He, J. and N. L. Oleinick (1995). Cell death mechanisms vary with photodynamic therapy dose and photosensitizer. 5th International Photodynamic Association Biennial Meeting

43. Helm, I., L. Jalukse, et al. (2009). "Micro-Winkler titration method for dissolved oxygen concentration measurement." Anal Chim Acta 648(2): 167-173.

44. Henderson, B. W. and V. H. Fingar (1987). "Relationship of tumor hypoxia and response to photodynamic treatment in an experimental mouse tumor." Cancer Res 47(12): 3110-3114.

45. Henderson, L. M. and J. B. Chappell (1993). "Dihydrorhodamine 123: a fluorescent probe for superoxide generation?" Eur J Biochem 217(3): 973-980.

46. Hoe, S., D. A. Rowley, et al. (1982). "Reactions of ferrioxamine and desferrioxamine with the hydroxyl radical." Chem Biol Interact 41(1): 75-81.

47. Indo, H. P., M. Davidson, et al. (2007). "Evidence of ROS generation by mitochondria in cells with impaired electron transport chain and mitochondrial DNA damage." Mitochondrion 7(1-2): 106-118.

48. Kessel, D. (2004). "Correlation between subcellular localization and photodynamic efficacy." J Porphyr Phthalocyanines 08(08): 1009-1014.

49. Kessel, D. (2008). "Promotion of PDT efficacy by a Bcl-2 antagonist." Photochem Photobiol 84(3): 809-814.

50. Kessel, D. and A. S. Arroyo (2007). "Apoptotic and autophagic responses to Bcl-2 inhibition and photodamage." Photochem Photobiol Sci 6(12): 1290-1295.

51. Kessel, D., Y. Luo, et al. (1997). "The role of subcellular localization in initiation of apoptosis by photodynamic therapy." Photochem Photobiol 65(3): 422-426.

52. Kessel, D. and N. L. Oleinick (2009). "Initiation of autophagy by photodynamic therapy." Methods Enzymol 453: 1-16.

53. Kessel, D. and M. Price (2012). PDT: loss of autophagic cytoprotection after lysosomal photodamage, SPIE.

54. Kessel, D., M. Price, et al. (2012). "ATG7 deficiency suppresses apoptosis and cell death induced by lysosomal photodamage." Autophagy 8(9).

55. Kim, H. R., Y. Luo, et al. (1999). "Enhanced apoptotic response to photodynamic therapy after bcl-2 transfection." Cancer Res 59(14): 3429-3432.

56. Kim, J., M. E. Rodriguez, et al. (2008). "Oxidative modification of cytochrome c by singlet oxygen." Free Radic Biol Med 44(9): 1700-1711.

57. Kobayashi, S., M. Nakano, et al. (1987). "On the mechanism of the peroxidase-

catalyzed oxygen-transfer reaction." Biochemistry 26(16): 5019-5022.

58. Koepke, J. I., K. A. Nakrieko, et al. (2007). "Restoration of peroxisomal catalase import in a model of human cellular aging." Traffic 8(11): 1590-1600.

59. Kohler, H. and H. Jenzer (1989). "Interaction of lactoperoxidase with hydrogen peroxide. Formation of enzyme intermediates and generation of free radicals." Free Radic Biol Med 6(3): 323-339.

60. Kroemer, G. and B. Levine (2008). "Autophagic cell death: the story of a misnomer." Nat Rev Mol Cell Biol 9(12): 1004-1010.

61. Levine, B. and D. J. Klionsky (2004). "Development by self-digestion: molecular mechanisms and biological functions of autophagy." Dev Cell 6(4): 463-477.

62. Luo, J., L. Li, et al. (2006). "Inactivation of primary antioxidant enzymes in mouse keratinocytes by photodynamically generated singlet oxygen." Antioxid Redox Signal 8(7-8): 1307-1314.

63. Luo, Y. and D. Kessel (1997). "Initiation of apoptosis versus necrosis by photodynamic therapy with chloroaluminum phthalocyanine." Photochem Photobiol 66(4): 479-483.

64. Marchal, S., A. Francois, et al. (2007). "Relationship between subcellular localisation of Foscan and caspase activation in photosensitised MCF-7 cells." Br J Cancer 96(6): 944-951.

65. Mazor, O., A. Brandis, et al. (2005). "WST11, a novel water-soluble bacteriochlorophyll derivative; cellular uptake, pharmacokinetics, biodistribution and vascular-targeted photodynamic activity using melanoma tumors as a model." Photochem Photobiol 81(2): 342-351.

66. McMahon, K. S., T. J. Wieman, et al. (1994). "Effects of photodynamic therapy

using mono-L-aspartyl chlorin e6 on vessel constriction, vessel leakage, and tumor response." Cancer Res 54(20): 5374-5379.

67. Moan, J. and K. Berg (1991). The photodegradation of porphyrins in cells can be used to estimate the lifetime of singlet oxygen. Photochem Photobiol 53(4):549-553.

68. Moan, J. and Q. Peng (2003). An outline of the history of PDT. Photodynamic Therapy. T. Patrice.

69. Moan, J. and S. Sommer (1985). "Oxygen dependence of the photosensitizing effect of hematoporphyrin derivative in NHIK 3025 cells." Cancer Res 45(4): 1608-1610.

70. Moan, J. and E. Wold (1979). "Detection of singlet oxygen production by ESR." Nature 279(5712): 450-451.

71. Moeller, B. J., R. A. Richardson, et al. (2007). "Hypoxia and radiotherapy: opportunities for improved outcomes in cancer treatment." Cancer Metastasis Rev 26(2): 241-248.

72. Moulder, J. E. and S. Rockwell (1987). "Tumor hypoxia: its impact on cancer therapy." Cancer Metastasis Rev 5(4): 313-341.

73. Niziolek-Kierecka, M., A. Pilat, et al. (2010). "Apoptosis-accommodating effect of nitric oxide in photodynamically stressed tumor cells." Photochem Photobiol 86(3): 681-686.

74. Nunez, G., M. A. Benedict, et al. (1998). "Caspases: the proteases of the apoptotic pathway." Oncogene 17(25): 3237-3245.

75. Oleinick, N. L., R. L. Morris, et al. (2002). "The role of apoptosis in response to photodynamic therapy: what, where, why, and how." Photochem Photobiol Sci 1(1): 1-21.

76. Oliveira, M. S., D. Severino, et al. (2011). "Singlet molecular oxygen trapping by the fluorescent probe diethyl-3,3'-(9,10-anthracenediyl)bisacrylate synthesized by the Heck reaction." Photochem Photobiol Sci 10(10): 1546-1555.

77. Pattingre, S. and B. Levine (2006). "Bcl-2 inhibition of autophagy: a new route to cancer?" Cancer Res 66(6): 2885-2888.

78. Peng, T. I., C. J. Chang, et al. (2005). "Mitochondrion-targeted photosensitizer enhances the photodynamic effect-induced mitochondrial dysfunction and apoptosis." Ann N Y Acad Sci 1042: 419-428.

79. Plaetzer, K., B. Krammer, et al. (2009). "Photophysics and photochemistry of photodynamic therapy: fundamental aspects." Lasers Med Sci 24(2): 259-268.

80. Price, M. and D. Kessel (2010). "On the use of fluorescence probes for detecting reactive oxygen and nitrogen species associated with photodynamic therapy." J Biomed Opt 15(5): 051605.

81. Price, M., J. J. Reiners, et al. (2009). "Monitoring singlet oxygen and hydroxyl radical formation with fluorescent probes during photodynamic therapy." Photochem Photobiol 85(5): 1177-1181.

82. Qin, Y., M. Lu, et al. (2008). "Dihydrorhodamine 123 is superior to 2,7-dichlorodihydrofluorescein diacetate and dihydrorhodamine 6G in detecting intracellular hydrogen peroxide in tumor cells." Cell Biol Int 32(2): 224-228.

83. Reiners, J. J., Jr., J. A. Caruso, et al. (2002). "Release of cytochrome c and activation of pro-caspase-9 following lysosomal photodamage involves Bid cleavage." Cell Death Differ 9(9): 934-944.

84. Robertson, C. A., D. H. Evans, et al. (2009). "Photodynamic therapy (PDT): a short review on cellular mechanisms and cancer research applications for PDT."

J Photochem Photobiol B 96(1): 1-8.

85. Runnels, J. M., N. Chen, et al. (1999). "BPD-MA-mediated photosensitization in vitro and in vivo: cellular adhesion and beta1 integrin expression in ovarian cancer cells." Br J Cancer 80(7): 946-953.

86. Saran, M. and K. H. Summer (1999). "Assaying for hydroxyl radicals: hydroxylated terephthalate is a superior fluorescence marker than hydroxylated benzoate." Free Radic Res 31(5): 429-436.

87. Scherz-Shouval, R., E. Shvets, et al. (2007). "Oxidation as a post-translational modification that regulates autophagy." Autophagy 3(4): 371-373.

88. Setsukinai, K., Y. Urano, et al. (2003). "Development of novel fluorescence probes that can reliably detect reactive oxygen species and distinguish specific species." J Biol Chem 278(5): 3170-3175.

89. Shannon, A. M., D. J. Bouchier-Hayes, et al. (2003). "Tumour hypoxia, chemotherapeutic resistance and hypoxia-related therapies." Cancer Treat Rev 29(4): 297-307.

90. Sibata, C. H., V. C. Colussi, et al. (2000). "Photodynamic therapy: a new concept in medical treatment." Braz J Med Biol Res 33(8): 869-880.

91. Spikes, J. D. and J. C. Bommer (1993). "Photobleaching of mono-L-aspartyl chlorin e6 (NPe6): a candidate sensitizer for the photodynamic therapy of tumors." Photochem Photobiol 58(3): 346-350.

92. Spikes, J. D. and J. C. Bommer (1993). "Photosensitizing properties of mono-L-aspartyl chlorin e6 (NPe6): a candidate sensitizer for the photodynamic therapy of tumors." J Photochem Photobiol B 17(2): 135-143.

93. Storrie, B. and E. A. Madden (1990). "Isolation of subcellular organelles."

Methods Enzymol 182: 203-225.

94. Sumitomo, K., N. Shishido, et al. (2007). "Effects of MCI-186 upon neutrophil-derived active oxygens." Redox Rep 12(4): 189-194.

95. Tada-Oikawa, S., S. Oikawa, et al. (2009). "DNA damage and apoptosis induced by photosensitization of 5,10,15,20-tetrakis (N-methyl-4-pyridyl)-21H,23H-porphyrin via singlet oxygen generation." Photochem Photobiol 85(6): 1391-1399.

96. Teicher, B. A. (1994). "Hypoxia and drug resistance." Cancer Metastasis Rev 13(2): 139-168.

97. Terlecky, S. R. and J. I. Koepke (2007). "Drug delivery to peroxisomes: employing unique trafficking mechanisms to target protein therapeutics." Adv Drug Deliv Rev 59(8): 739-747.

98. Terlecky, S. R., J. I. Koepke, et al. (2006). "Peroxisomes and aging." Biochim Biophys Acta 1763(12): 1749-1754.

99. Thomas, J. P., R. D. Hall, et al. (1987). "Singlet oxygen intermediacy in the photodynamic action of membrane-bound hematoporphyrin derivative." Cancer Lett 35(3): 295-302.

100. Tyrrell, R. M. and M. Pidoux (1989). "Singlet oxygen involvement in the inactivation of cultured human fibroblasts by UVA (334 nm, 365 nm) and near-visible (405 nm) radiations." Photochem Photobiol 49(4): 407-412.

101. Verma, S., G. M. Watt, et al. (2007). "Strategies for enhanced photodynamic therapy effects." Photochem Photobiol 83(5): 996-1005.

102. Wasil, M., B. Halliwell, et al. (1987). "The specificity of thiourea, dimethylthiourea and dimethyl sulphoxide as scavengers of hydroxyl radicals. Their protection of

alpha 1-antiproteinase against inactivation by hypochlorous acid." Biochem J 243(3): 867-870.

103. Wei, H., Q. Cai, et al. (1997). "Singlet oxygen involvement in ultraviolet (254 nm) radiation-induced formation of 8-hydroxy-deoxyguanosine in DNA." Free Radic Biol Med 23(1): 148-154.

104. Weishaupt, K. R., C. J. Gomer, et al. (1976). "Identification of singlet oxygen as the cytotoxic agent in photoinactivation of a murine tumor." Cancer Res 36(7 PT 1): 2326-2329.

105. Wirawan, E., T. Vanden Berghe, et al. (2012). "Autophagy: for better or for worse." Cell Res 22(1): 43-61.

106. Xue, L. Y., S. M. Chiu, et al. (2008). "Protection by Bcl-2 against apoptotic but not autophagic cell death after photodynamic therapy." Autophagy 4(1): 125-127.

107. Xue, L. Y., S. M. Chiu, et al. (2001). "Photochemical destruction of the Bcl-2 oncoprotein during photodynamic therapy with the phthalocyanine photosensitizer Pc 4." Oncogene 20(26): 3420-3427.

108. Yang, Z. and D. J. Klionsky (2009). "An Overview of the Molecular Mechanism of Autophagy." Curr Top Microbiol Immunol 335: 1-32.

109. Zhao, H., S. Kalivendi, et al. (2003). "Superoxide reacts with hydroethidine but forms a fluorescent product that is distinctly different from ethidium: potential implications in intracellular fluorescence detection of superoxide." Free Radic Biol Med 34(11): 1359-1368.

110. Zielonka, J. and B. Kalyanaraman (2010). "Hydroethidine- and MitoSOX-derived red fluorescence is not a reliable indicator of intracellular superoxide formation: another inconvenient truth." Free Radic Biol Med 48(8): 983-1001.

ABSTRACT

A ROLE FOR REACTIVE OXYGEN SPECIES IN PHOTODYNAMIC THERAPY

by

MICHAEL PRICE

December 2012

Advisor: David Kessel, Ph.D.

Major: Cancer Biology

Degree: Doctor of Philosophy

Photodynamic therapy (PDT) is based on the ability of certain photosensitizing agents to selectively localize in neoplastic cells and their vasculature. Subsequent irradiation at a wavelength corresponding to a photosensitizer absorbance band excites the photosensitizer molecules, leading to energy transfer reactions and fluorescence. It was initially concluded that the phototoxic effect occurred when energy from the excited state of the photosensitizer was transferred to dissolved oxygen to form singlet oxygen. This product has a very brief half-life and will cause cellular damage only in the immediate vicinity of its formation. But an excited-state photosensitizer can also interact with oxygen to form superoxide anion radical, which in turn (through the action of superoxide dismutase) is converted to hydrogen peroxide and hydroxyl radical via the Fenton reaction. These reactive oxygen species (ROS) all posses properties (i.e. lifetime, reactivity and diffusion distances) that make them at least as cytotoxic as singlet oxygen. The hypothesis examined in this dissertation was that the particular reactive oxygen species being formed might be an important determinant of photodynamic therapy efficacy.

Initial studies were designed to assess specificity of several commercially

available fluorogenic probes that could used for identification of ROS generated during PDT. APF (for hydroxyl radical) and DADB (for singlet oxygen) were found to be useful for cell culture studies in the context of PDT while other probes were found to have less specificity than advertised.

Using an inhibitor of catalase (3-AT) and an endogenous source of catalase that localizes to peroxisomes (termed CAT_{SKL}) it was feasible to alter the level of hydrogen peroxide produced by PDT. Promoting persistence of hydrogen peroxide resulted in enhanced photokilling and vice versa. This indicates a role for hydrogen peroxide and its downstream product in the photokilling process.

The efficacy of singlet oxygen generation vs. oxygen radicals was then compared. The photosensitizer NPe6 localizes in lysosomes and generates singlet oxygen in a high yield. The photosensitizer WST11 also localized in lysosomes, and has been reported to produce only oxygen radicals upon irradiation under aqueous conditions. This was confirmed by studies using the singlet oxygen probe DADB. The efficacy of these photosensitizers was compared under conditions where the oxygenation level was varied. In cell culture, lowering the oxygenation levels from 20% to 1% did not alter the phototoxicity of NPe6. WST11 phototoxicity was reduced in the 1% oxygen.

In a cell-free system, the initial rate of formation of singlet oxygen from NPe6 was independent of the oxygen content. For both NPe6 and WST11, formation of hydroxyl was, however, highly correlated with the level of oxygenation.

These data indicate important roles for several different ROS that can be formed during PDT. With most common photosensitizing agents, effects of singlet oxygen generally predominate, especially under hypoxic conditions, but in a well-oxygenated

system, formation of hydrogen peroxide and hydroxyl radical can also promote lethal photodamage. The photosensitizing agent WST11 represents a possibly unique situation, where only hydroxyl radical is involved in photobleaching and tumor eradication.

AUTOBIOGRAPHICAL STATEMENT

MICHAEL PRICE

EDUCATION

2001-2005 Bachelor of Science, Alma College, Alma, MI

2005-2012 Doctor of Philosophy in Cancer Biology, Wayne State University

HONORS AND AWARDS

PUBLICATIONS

1. Kessel, D., **Price, M**., & Reiners, J. J., Jr. (2008). The Bcl-2 antagonist HA14-1 forms a fluorescent albumin complex that can be mistaken for several oxidized ROS probes. *Photochem Photobiol, 84*(5), 1272-1276.
2. **Price, M**., Reiners, J. J., Santiago, A. M., & Kessel, D. (2009). Monitoring singlet oxygen and hydroxyl radical formation with fluorescent probes during photodynamic therapy. *Photochem Photobiol, 85*(5), 1177-1181.
3. **Price, M**., Terlecky, S. R., & Kessel, D. (2009). A role for hydrogen peroxide in the pro-apoptotic effects of photodynamic therapy. *Photochem Photobiol, 85*(6), 1491-1496.
4. **Price, M**., & Kessel, D. (2010). On the use of fluorescence probes for detecting reactive oxygen and nitrogen species associated with photodynamic therapy. *J Biomed Opt, 15*(5), 051605.
5. Andrzejak, M., **Price, M**., & Kessel, D. H. (2011). Apoptotic and autophagic responses to photodynamic therapy in 1c1c7 murine hepatoma cells. *Autophagy, 7*(9), 979-984.
6. Kessel, D., **Price, M**., Caruso, J., & Reiners, J., Jr. (2011). Effects of photodynamic therapy on the endocytic pathway. *Photochem Photobiol Sci, 10*(4), 491-498.
7. Kessel, D., & **Price, M**. (2012). Evaluation of Diethyl-3-3'-(9,10-anthracenediyl)bis Acrylate as a Probe for Singlet Oxygen Formation during Photodynamic Therapy. *Photochem Photobiol*.
8. Kessel, D. H., **Price, M**., & Reiners, J. J., Jr. (2012). ATG7 deficiency suppresses apoptosis and cell death induced by lysosomal photodamage. *Autophagy, 8*(9).